Laboratory of Geo-Information Science and Remote Sensing

Thesis Report GIRS-2016-23

Detection of tropical forest canopy gaps caused by selective logging using hyperspectral remote sensing

Lazaros Spaias

August 2016

WAGENINGEN UNIVERSITY
WAGENINGEN UR

Detection of tropical forest canopy gaps caused by selective logging using hyperspectral remote sensing

Lazaros Spaias

Registration number 891202788060

<u>Supervisors</u>:

Dr. Juha Suomalainen

Jose Gonzalez de Tanago

A thesis submitted in partial fulfilment of the degree of Master of Science

at Wageningen University and Research Centre,

The Netherlands.

August 2016

Wageningen, the Netherlands

Abstract

The aim of this research is to assess the detectability of small spatial scale selective logging in tropical forests using optical very high spatial and spectral resolution data. Among the forest change processes contributing to the global greenhouse gas emissions, the degradation processes like selective logging represent the most challenging ones to be detected and quantified due to their partial forest canopy removal and their small scale. Furthermore selective logging events are considered as precursor of deforestation and important drivers for reduction of ecosystem services provided by tropical forests. In this research an Unmanned Airborne Vehicle (UAV) with a hyperspectral camera was used to detect small scale canopy gaps originating from selective logging in the tropical regions of Guyana and Indonesia. The UAV-based radiometric detection analysis provides the possibility to calibrate and validate a selective logging radiometric detection method based on airborne or satellite-borne very high spatial resolution data. The data consists of hyperspectral, Digital Surface Model (DSM) images and photos from a commercial camera (RGB). Two flights, a pre-harvest and a post-harvest flight performed with a tree harvested in between on each plot. With the UAV derived DSM and RGB images, the newly created canopy gaps were firstly visually identified. Then their spectral characteristics were explored using the hyperspectral data-cube. Three types of gaps were identified according to their spectral properties, the "*Shadowed gap*", the "*Non Photosynthetic Vegetation (NPV)-Soil gap*", and the "*Understory gap*". Using spectral unmixing (SMACC algorithm), abundance maps were derived. Depending on the type of gap, the corresponding endmember was loaded. A subtraction between the pre- and post-harvest datasets revealed the area that the logging event affected. It was found that the "*Understory gap*" was the hardest to detect due to its small size and spectral variability. Finally, a detectability analysis gave insight on how much area should the gap cover in a pixel in order to be detected. The Signal to Noise Ratio (SNR) was set at 10 as a threshold to distinguish the change over the background of the image. The analysis showed that the required sub-pixel gap area for detection is 68% for *"Shadowed gaps",* 89% for "*NPV-Soil gap*", and 100% sub-pixel gap area for *"Understory gap"*. The gap sizes found in this study were 189 m^2 for "*Shadowed gaps*", 79 m^2 for "*NPV-Soil gap*", and 51 m^2 for "*Understory gap*". Finally, the hyperspectral pixel size required for detection was calculated combining the sub-pixel gap area and the gap size of each gap type found in this study. The pixel sizes were defined as: 9.3x9.3 m^2 for "*Shadowed gap*", 7x7 m^2 for "*NPV-Soil gap*", and 1x1 m^2 for "*Understory gap*". However the pixel size represents only the gaps studied in this research.

Keywords: Tropical forest, Selective logging, Canopy gap, UAV, Spectral Unmixing

Table of Contents

List of figures

List of tables

Abbreviations

FAO	Food and Agriculture Organization
REDD+	Reducing Emissions from Deforestation and forest Degradation on developing countries, and the role of conservation, sustainable management of forests, and enhancement of forest carbon stocks in developing countries
RIL	Reduce Impact Logging
TM	Thematic Mapper
MTMF	Mixture-Tuned Matched Filtering
NIR	Near Infra-Red
SAR	Synthetic Aperture Radar
LiDAR	Laser Imaging Detection And Ranging
NDFI	Normalized Difference Fraction Index
SMA	Spectral Mixture Analysis
UAV	Unmanned Aerial Vehicle
HYMSY	HYperspectral Mapping SYstem
GPS-INS	Global Positioning System-Inertial Navigation System
RGB	Red Green BLue
DSM	Digital Surface Model
NPV	Non Photosynthetic Vegetation
ASCII	Acronym for the American Standard Code for Information Interchange
GeoTIFF	Geo- Tagged Image File Format
SMACC	Sequential Maximum Angle Cone Convex
ROI	Region Of Interest
S/N	Signal to Noise ratio
GV	Green Vegetation

Chapter 1: Introduction

The degradation in tropical forests is receiving a growing attention by scientists and policy makers over the last years. Data are needed in order to plan and apply a forest oriented policy to control, quantify, and qualify the degradation (FAO, 2011a). According to Food and Agriculture Organization FAO (2010a), forest degradation can be defined as: a gradient depletion of the ability of a forest to supply with goods and services. This definition can be interpreted in many different ways, depending on the nature of the degradation, for example: forest health and vitality, biological diversity, protective functions of forest resources, productive functions of forest resources and, socio-economic functions of forests (FAO, 2011a).

Moreover, the climate change policies in the context of REDD+ (*reducing emissions from deforestation and forest degradation, conservation of existing forest carbon stocks, sustainable management of forests and, enhancement of forest carbon stocks*) are interested in the emissions that are caused from forest degradation (Romijn 2013). In this framework, forest degradation is defined as the negative human influence to the forest's carbon stock in areas that forests remain forests, meaning that their values and properties persist over the boundaries of what is defined as forest (Herold and Skutsch 2011).

In rainforests and specifically in Indonesia which is one of the two study areas there are multiple drivers pushing forests to degrade such as: shifting cultivation, fuel wood collection, wood extraction for charcoal production, legal and illegal selective logging, and more (Miettinen et al., 2014). There have been reports that selective logging is been practiced in large areas of Southeast Asia since the mid of the 19th Century (Schlich, 1907). When selective logging is practiced in a sustainable way it does not lead to forest degradation (Miettinen et al., 2014). On the other hand, selective logging practiced in an unsustainable way can lead to forest degradation (Mon et al., 2012a), and according to Kissinger et al. (2012) is the leading driver of forest degradation in these areas. In Southeast Asia the main reasons for forest degradation are shifting cultivation, fire, and selective logging (Stibig et al. 2007b). Particularly, in the islands of Southeast Asia (Malaysia, Singapore, Brunei, East Timor, Indonesia, and the Philippines) (Miettinen et al., 2014), the logging activities due to the valuable tree species and also because these countries are not practicing the Reduced Impact Logging (RIL) (FAO, 2011b), are more intense than in other

tropical regions (Miettinen et al., 2014). Moreover, short rotational logging times such as 20 years (Wilcove et al., 2013) are adding to the unsustainable logging practices resulting in a biomass reduction cycle (Miettinen et al., 2014).

1.1 Literature Review

Traditionally the forest canopy gaps where characterized through field surveys (Brokaw & Grear 1991). For larger and wider areas where the field methods are limited (Runkle 1982), remote sensing found to be cheaper and less labor intensive (Woodcock et al., 2001).

Various techniques to map forest degradation from selectively logged areas have been developed for different study areas. Visual interpretation using images from Landsat Thematic Mapper (TM) to characterize selective logging was tested by (Stone and Lefebvre, 1998). The authors managed to measure the logged areas under the condition that the image is acquired in a short period after the logging. Due to Landsat's TM coarse resolution (30x30m), this method is feasible only when the logging areas are at least as big as the pixel size (Souza et al., 2005). Moreover, visual interpretation is subjective and labor intensive when it comes to large areas (Mietinen et al., 2014). Negron-Juarez et al. (2011) and Asner et al. (2004) also used Landsat images to map selective logging but with the 30x30m area limitation to remain.

Minimum distance and maximum likelihood classification (Stone & Lefebvre, 1998) was used in Amazonia to classify selectively logged areas using Landsat TM satellite data. This approach was not capable to define a different spectral class for selectively logged areas due to the complexity of the forest's structure, the coarse resolution of the sensor, and the cloud coverage in the area. The authors stated that an automated classification procedure to detect the logging areas is unlikely to be developed under this setting. Reflectance and texture analysis (Asner et al., 2002a) have also been used for mapping selective logging but without robust results due to Landsat's spectral and spatial limitations. The difficulty lies due to the fact that gaps that are formed by selective logging are small and therefore very difficult to detect with Landsat.

Franke et al (2012) used multi-temporal Rapid Eye satellite data in Southern Kalimantan, Indonesia and they were able to apply Mixture-Tuned Matched Filtering (MTMF), a linear spectral unmixing technique to detect areas that were disturbed by unplanned (illegal) logging. Malahlela et al (2014) used WorldView-2 data to detect gaps in a subtropical forest with dense vegetation in South Africa. They used two classification techniques, the pixel based (Maximum likelihood, Support Vector Machine, and Random Forest) and the object-

2

based image analysis. Both methods succeed higher accuracy compared to sensors with the conventional visible and Near-Infrared (NIR) bands. However this paper outlines that these methods are still inferior to the methods that are using Light Detection And Ranging (LiDAR) technology and this is because laser scanners can also capture tree height where the traditional optical sensors cannot (Dubayah and Drake 2000; Harding et al. 2001; Nelson, Oderwald and Gregoire 1997).

However, the costs and the data dimensionality of the LiDAR technology are high (Mutanga, Adam and Cho 2012) and therefore its application especially in large areas with dense revisit times is limited. Gong, Biging and Standiford 2000, Swellengrebel 1959, and Green 2000 used digital aerial photography and digital surface models to map canopy gaps with success. Depending on the application, aerial photography has some disadvantages because it is time consuming and their availability for tropical areas is limited (Asner et al., 2002b). Canopy gaps where also derived using Synthetic Aperture Radar (SAR) interferometry (Ferrazoli and Guerriero 1994; Imhoff 1995) but with the same practical limitations as LiDAR scanners (Malahlela et al., 2014).

Some methods that were developed for the Amazon basin could possibly be used in other tropical regions. Some examples of these methods are: segmentation based automated statistical method for gap detection (Pithon et al., 2013) and combination of Spectral Mixture Analysis (SMA) information into one band, using the Normalized Difference Fraction Index (NDFI) to detect forest areas with canopy damage (Souza et al. 2005).

1.2 Problem Definition

In our study areas, forests in their non-affected state have closed canopies. A forest with closed canopy makes simpler the degradation monitoring because areas with gaps and reduced canopy cover can be counted as a sign of selective logging activity (Miettinen et al., 2014). Furthermore, the climate conditions result in small yearly variations of forest features making the detection less complex (Miettinen et al., 2014). However, even with the aforementioned detection advantages of the tropical forests, the mapping of selective logging using optical remote sensing remains hard since the cloudy climatic conditions and atmospheric disturbances make the acquisition of suitable satellite images difficult (Miettinen et al., 2014). Moreover, the scale of the disturbance is small and variates in signal characteristics and thus hard to detect with conventional sensors. The fast regrowth of those forests makes the detection problematic because the traces of the gaps fade quickly. That results in low differentiation between gap and vegetated pixels (Miettinen et al., 2014).

1.3 Objectives

This research is focusing on the radiometric detection of canopy gaps that are created by selective logging in the tropics. The main objective is to develop a method to detect gaps caused by selective logging, through radiometric differences in high and very-high (5-10m) spatial resolution satellite imagery.

For achieving this, the following research questions have to be answered.

RQ1. What are the spectral characteristics of a canopy gap caused by selective logging in the tropics?

RQ2. Can selectively logged canopy gaps be detected by spectral unmixing of bi-temporal hyperspectral datasets?

RQ3. How big should the pixel be and how much subpixel area should the gap cover in order to be detectable?

Chapter 2: Study area and UAV data

2.1 Study Areas

The UAV data were collected in two study areas, covered by tropical forests: one in Indonesia, (Central Kalimantan) and one in Guyana, (South of Bartica).

2.1.1 Indonesia

The first study area (Figure 1) is located in Southern Central Kalimantan, Indonesia, and it lies between Latitude -2.40° and Longitude 113.13° (datum WGS84). The study area consists of peat swamp forests, which are moist forests with hard access due to their density and soil condition. The peat swamp forests occur where very wet soils do not let wood and dead leaves to decompose creating a "carpet" of acidic peat which can reach a 10-12m thickness.

In 1996 a project called Mega Rice Project was initiated in order to counter Indonesia's growing food shortage. The aim was to turn one million hectares of peat swamp forests into rice paddies. The project failed and was abandoned but causing significant damage to the ecosystem.

In the study area logging events and natural canopy gaps took place before the data acquisition creating openings in the canopy which were heterogeneously distributed in the

area. The peat swamp forests are well-known for their abundance in valuable trees. This leads to fast deforestation caused by legal or illegal logging (Nurhayati, 2015).

Three plots of 40x30m size each were stablished in a peat swamp forest area prior to selective logging operations. In each plot at least one major tree was logged. Geolocation of the tree logged and the plot boundaries was acquired with two hand held GPS averaging 1000 measurements for 13 locations on the boundaries of the plot and centre. Each tree with Diameter at Breast Height (DBH) larger than 10 cm was identified, labelled, measured its DBH, and its geolocation in a local relative coordinate system (in relation to one corner of the plot). Tree damage of each individual tree was assessed after the logging operation and canopy gap information was recorded.
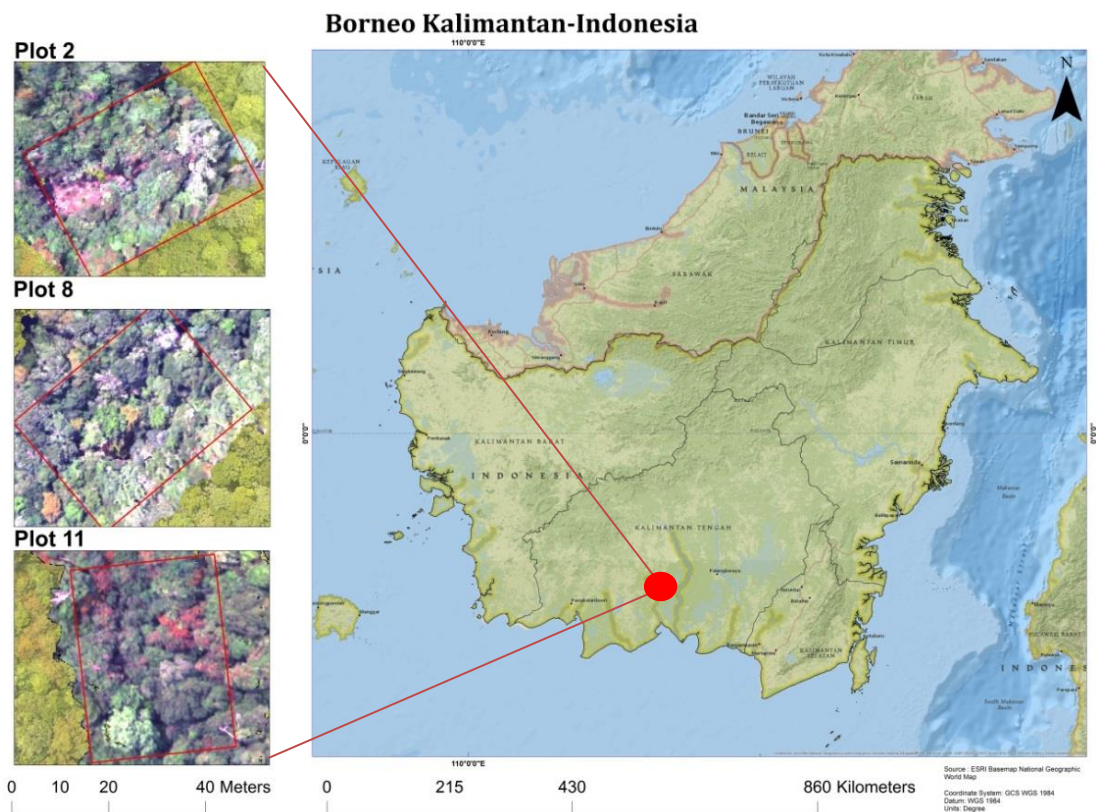
Figure 1. Location of the Indonesian plots. In the small rectangles are shown the RGB (larger extent greenish images) and Hyperspectral images (smaller extent area with distinct colors within the RGB image) acquired by the UAV. The red rectangles depict the delineated plot area where the logging event occurred.

2.1.2 Guyana

The study area is located in the forest of central Guyana, south of Bartica (Figure 2) and it lies between Latitude 6.33° and Longitude -58.62°. According to Ter Steege et al. (2002), the climate is wet with 2764mm/year rainfall with two dry seasons from January to March and August to September. The yearly mean daily temperature is 25 °C. In the study area, dry evergreen forest is the dominant forest type (Ter Steege et al., 2002). These types of forests cover 7% of the forested areas. Four plots of 40x30 m size each were used, plot 6, 7, 8 and 10.
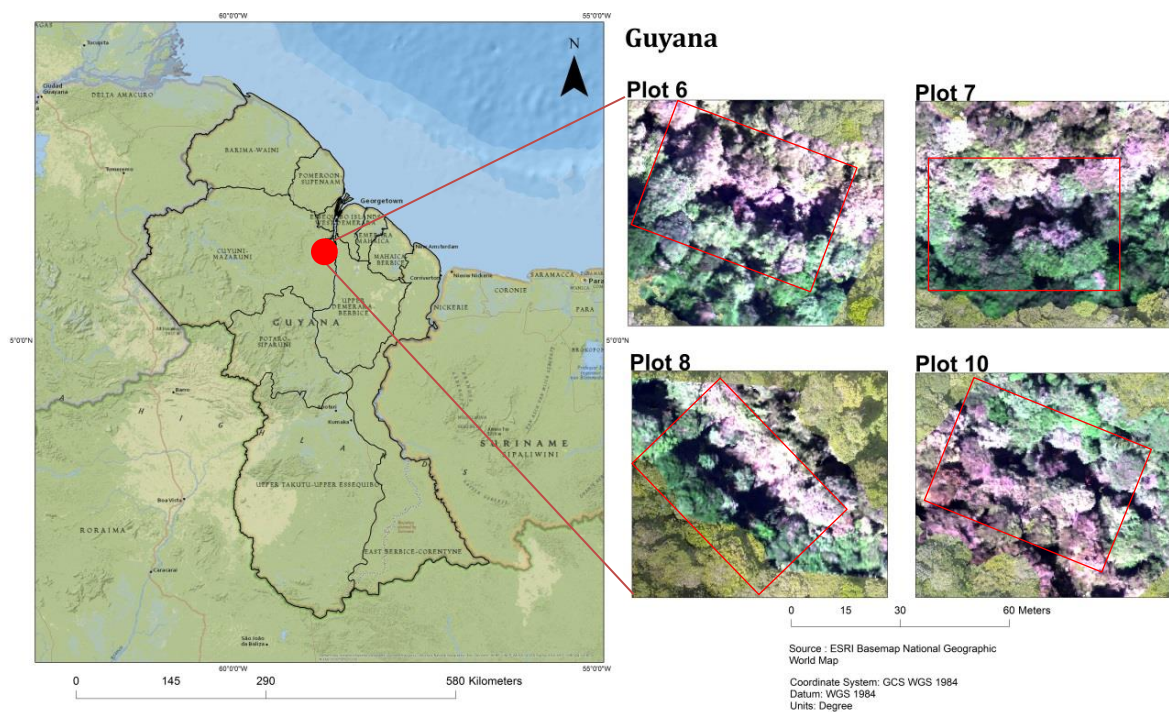
Figure 2. Location of the Guyanese plots. In the small rectangles are shown the RGB (larger extent greenish images) and Hyperspectral images (smaller extent area with distinct colors within the RGB image) acquired by the UAV. The red rectangles depict the delineated plot where the logging event occurred.

2.2 UAV data

The data were collected using a small lightweight (5kg when fully equipped) octocopter (Aerialtronics Altura AT8) equipped with the Hyperspectral Mapping System (HYMSY) (Figure 3) developed at Wageningen University, and a high spatial resolution RGB camera (20 cm) for ortho-photography. The HYMSY consists of a push-broom spectrometer, a consumer camera and a GPS-INS device. (Suomalainen et al., 2014).

Figure 3. The UAV mounted with the HYMSY

The spectrometer is able to derive 101 bands ranging from 450-950nm with 5nm intervals. The pixel size varied between the flights due to different flight altitude (Table 1).

Table 1. Plots and their corresponding pixel size

Study area and Plot number	Pixel Size (cm)
Indonesia 2	0.197
Indonesia 8	0.192
Indonesia 11	0.253
Guyana 6	0.215
Guyana 7	0.246
Guyana 8	0.211
Guyana 10	0.227

In this research, the RGB high resolution photos, the Digital Surface Model (DSM) derived from the orthophotogrammetry of the RGB imagery, and the hyperspectral datasets were used.

Each plot had the size of 40x30 meters. The plots were delineated using the main tree and its predicted falling direction to define the plot's orientation (Figure 4). The distance from the main tree to the closest plot edge was 10 meters for Indonesia and 5 meters for Guyana.
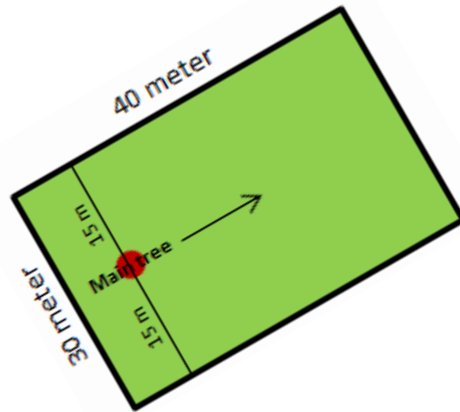
Figure 4. Schematic representation of the plot delineation. The arrow indicates the falling direction of the harvested tree

In order to study the canopy changes due to the selective logging events, two flights for each plot were carried out (**Error! Reference source not found.**). The first flight was to derive the pre-harvest (benchmark) dataset and the second flight to derive the post-harvest (logged) dataset. Between pre- and post-harvest flights a major size tree was logged creating a change in the canopy structure.
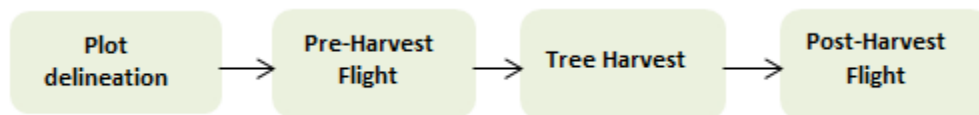
Figure 5. Generalized steps for the UAV data collection

Error! Reference source not found. shows the date and time of the pre- and post-harvest flights. Moreover, the solar zenith angle for each instance has been calculated. The solar angle is an important aspect of the data collection because if it is not consistent it can introduce differences in the shadowing effect between pre- and post-harvest flights.

These data have some unique characteristics that had to be taken into consideration before any further action. The mean flight height of the UAV was less than 100 meters. In this

altitude an atmospheric correction is not needed because it is assumed that the interference of the atmosphere is marginal. The sensor was calibrated before each flight using a white panel in order to calibrate for the illumination conditions. Finally, even with the UAV flying below the clouds, the image acquisition is still affected introducing shadows. However, in both the study areas, the flights where performed when no clouds blocking the sun.

Table 2. Date, time and solar zenith angle of pre- and post-harvest flights. The negative solar zenith angle in Guyanese plots means that the sun angle is west of south.

Study Area and Plot No.	Date-Flight time (local time)		Solar zenith angle °	
	Pre	Post	Pre	Post
Indonesia 2	17-08-2014 16:17	27-08-2014 17:09	13°	10°
Indonesia 8	02-09-2014 16:38	07-09-2014 17:12	8°	6°
Indonesia 11	08-09-2014 15:32	09-09-2014 16:50	5.5°	5°
Guyana 6	21-11-2014 14:32	23-11-2014 13:48	-20°	-20°
Guyana 7	21-11-2014 15:19	23-11-2014 15:36	-20°	-20°
Guyana 8	22-11-2014 15:36	30-11-14 16:41	-20°	-21°
Guyana 10	30-11-2014 14:20	30-11-2014 16:10	-21°	-21°

Chapter 3: Methods

The methodology was tested in 7 plots, 4 in Guyana and 3 in Indonesia. This research used only a subset of 7 out of the 20 plots where data acquired (Indonesia plot 2, 8, and 11; and Guyana plot 6, 7, 8, and 10) but the naming was kept the same for convenience. The datasets that were omitted did not fit the criteria for this research. In some of the omitted plots the pre-harvest datasets were missing and in other plots the pre and post-harvest datasets did not overlap meaning that the pre- and post-harvest dataset comparison would not be possible.

3.1 Forest canopy gap definition

There are many forest canopy gap definitions available in the literature (Oldeman, 1978 Runkle, 1981; Brokaw, 1982; Popma et al., 1988, Whitmore et al., 1993, Koukoulas and

Blackburn 2004). Oldeman (1978) defined them as openings in the forest canopy that are irregularly shaped and they do not have clear borders between the gap area and the closed forest. The definition by Oldeman is focusing on defining the gap's vertical and horizontal structure and its borders. In this research is important to consider gaps from a remote sensing point of view. Koukoulas and Blackburn (2004) stated that gaps are ecological features that have optical properties. After a gap is created, changes affect the structure of the canopy and the radiation reflected from the forest in the logged area (Koukoulas and Blackburn 2004). This characteristic provides the theoretical background under which passive optical remote sensing can be used for the study of gaps. (Koukoulas and Blackburn 2004).

For the scope of this research, a gap is used as a proxy for detection of potential selective logging event occurred in an area via comparing bi-temporal remote sensing images. A gap is considered as the area that is affected during a selective logging event.

Based on their optical characteristics, three gap types were distinguished (Figure 6). "*NPV-Soil gap*" is the type of gap where a mixture of soil and Non-Photosynthetic-Vegetation (NPV) is exposed after the logging. "*Shadowed gap*" is the type of gap characterized by an increase in shadow in the area after the tree harvest. In this occasion the harvested tree affects the canopy creating a gap but this gap is shadowed and NPV or soil could not be spotted. This can be explained by the solar angle, the density of the forest, the size of the harvested tree etc. Finally, "*Understory gap*" is the type of gap where understory vegetation is exposed after the tree harvest. This type does not fit the gap definitions found in the literature because after the harvest there is not a ground reaching opening in the canopy. Still, in this research it is known that a tree was harvested and it did not create a gap so it is interesting to try and detect the selectively logged affected area, even if the harvest did not create a "traditional" gap.

The "*Understory gap*" has similarities with the "*Shadowed gap*" such as the increase in shadow after the tree removal. However, it is relevant to introduce this gap category separately from the "*Shadowed gap*" because of the secondary vegetation that is exposed after the harvest and not a clear shadowed area. With a visual assessment the logged area appears intact as nothing changed. However, the analysis showed that a subtle change in shadow occurred after the logging. Hence, the spectral characteristic that is used to detect the "Understory gap" is the shadow. Still, the term "*Understory gap*" is used in order to

underline that this change is very subtle and difficult to detect because spectrally the difference is very small.

Figure 6. Example of gap types as they are visualized in the hyperspectral datasets The selected RGB composite corresponds to a wavelength of 665nm (red), 565nm (green), and 465nm (blue). "*NPV-Soil gap*" (left), "*Shadowed gap*" (middle), and "*Understory gap*" (right)

3.2 Method for spectral characterization of canopy gaps (RQ1)

To answer research question 1 the following steps were implemented (Figure 7).
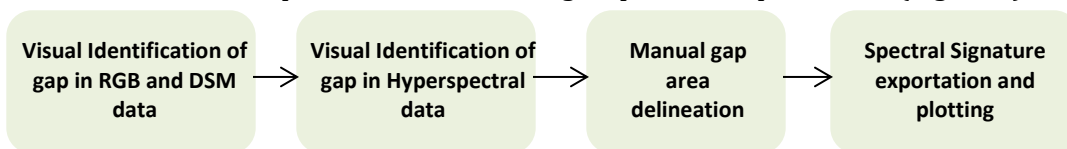
Figure 7. Workflow to derive the spectral characteristics of the gaps

Visual identification using only the hyperspectral data was hard due to the small scale of the change. Comparing the pre and post-harvest DSM (Figure 8) and RGB datasets made the identification easier. After the visual detection, the logged area was delineated from the hyperspectral datasets using ENVI version 5.3 (Exelis Visual Information Solutions, Boulder, Colorado*)*. The hyperspectral datasets were used for the delineation because the delineation of the logged area using the RGB or DSM dataset would include details that in the lower resolution hyperspectral data will disappear. Furthermore, the hyperspectral dataset is the one that the spectral signature of the gap was extracted from so the delineation should be based in this dataset in order to include only the pixels that represent the gap area. After the delineation, the next step is to export the mean value of all the pixels contained in the gap area to an ASCII file. Finally, the files were imported into an Excel spreadsheet for plotting.

11
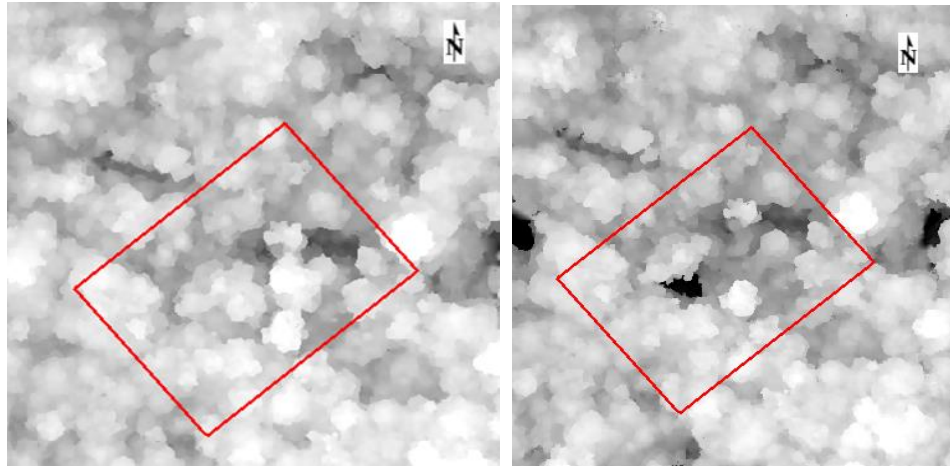
Figure 8. DSM dataset used for visual gap identification, pre (left) and post-harvest (right) in Indonesia, plot 2. The red rectangle represents the delineated plot

3.3 Method for radiometric detection of selective logging (RQ2)

The steps followed in order to answer the second research question are presented in (Figure 9. Workflow developed to answer the second research question). A spectral unmixing approach was chosen for two reasons. Firstly, the method should be able to apply in high -very high spatial resolution (5m-10m) satellites. Even with 5m pixel size the satellite might not be able to "catch" the subtle changes the selective logging event created. A spectral unmixing approach should solve this problem and derive information in a sub-pixel level. Secondly, the UAV data have high spectral resolution which is an advantage for spectral unmixing algorithms because the detailed spectral signature curve helps to distinguish between similar endmembers.
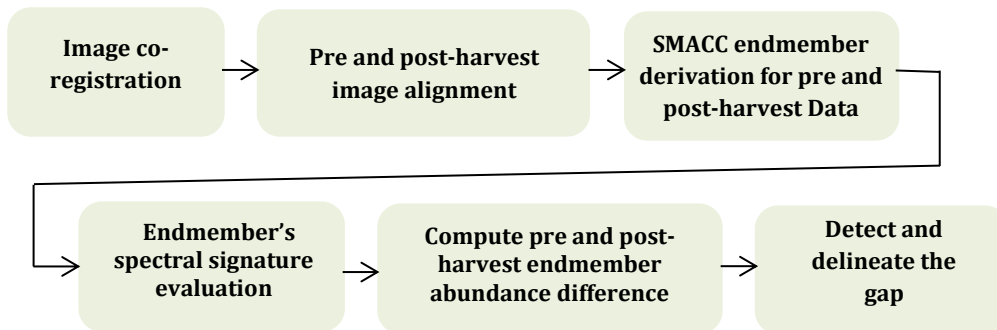
Figure 9. Workflow developed to answer the second research question

3.3.1 Image registration Workflow

The accuracy of the GPS mounted on the UAV produced a spatial offset between the pre- and post-harvest data, implying that co-registration is needed before further analysis. The co-registration will make sure that the corresponding pixels represent the same object. The co-registration was performed using ENVI's version 5.3 tool "*Image registration workflow*".

The pre-harvest dataset was used as a base image and the post-harvest as a warp image. Seed tie points were provided by the user in order to improve the accuracy of the automated tie point generation. The tie points were used by the algorithm to compute the parameters of the geometric transformation between the two datasets. The tie points are also used by the algorithm to align and resample the warp image in a way that matches the base image. Cross correlation was used as a matching method for the automated tie point generation because both the images were optical images. The minimum matching score which filters tie points based on a radiometric criterion was set at 0.7. This value is a fraction and it means that the matching window around the tie point in the warp image scored at least 0.7 when cross-correlated with the corresponding tie point of the base image. The "Fitting Global Transform" with a first-order polynomial transform was chosen as the geometric model and the maximum allowable error per tie point set at 0.5. This value represents the maximum error distance from the predicted tie point location. So, if the tie point exceeds this value then it's been omitted. Finally, the polynomial equation was chosen as warping parameter and nearest neighbor as resampling method.

3.3.2 Alignment of pre and post-harvest datasets

A necessary step before the analysis is to spatially align the images in a way that the extent of the pre and post-harvest datasets match. After the co-registration the two images still differ in extent and the pixels are not perfectly aligned. If they are not aligned then the comparison by subtraction will not be possible. The alignment forces the pixels of the two datasets to fall on top of each other. To do that an R script was used. The script is provided in Appendix A. The aligned datasets exported in a GeoTIFF format and loaded in ENVI version 5.3 where then the format changed into ENVI file format.

3.3.3 Spectral Unmixing using SMACC algorithm

The Sequential Maximum Angle Convex Cone (SMACC) is an automated endmember extraction method which can also derive each endmember's abundance in an image. Endmembers are spectral signatures that represent surface materials. The algorithm, finds the brightest pixel and then the pixel that is most different from the brightest. After, it searches for the pixel that is most different from the first two. This procedure continues until it finds the specified number of endmembers or find a pixel that already have been accounted for in the team of the previous pixels. A detailed explanation about the algorithm can be found in the paper of Gruninger et al. (2004).

For the scope of this research, 3 endmembers were defined: Vegetation, Shadow and Endmember 3. The Endmember 3 depending on the plot was either a mixture of NPV-Soil or vegetation that was differentiating from the dominant vegetation endmember. This approach was selected because at some plots the algorithm for the selected parameters could not distinguish an endmember for NPV-Soil but it could differentiate between different vegetation spectral signatures. The sum to unity constraint which is a constraint that dictates the sum of the fraction in a pixel to be 1 was chosen. According to the software's help documentation, this constraint is suggested when dark endmembers like shadow will included in the unmixing process. Finally, the RMS error tolerance was set at 0.2.

3.3.4 Endmember Assessment

As it was mentioned in the section 3.3.3, SMACC is an automated endmember detection and unmixing algorithm which means that it cannot receive spectral signature as endmember input in order to solve the unmixing equation. It is important to assess the derived endmembers in order to understand and be sure of what is the unmixing result. The resulted endmembers were exported to an excel file and plotted as a wavelength function. They were assessed plotting them with the observed spectral signatures. Moreover, a comparison between the pre and post-harvest endmember extraction is important in order to see if the viewing conditions and the co-registration errors introduced dissimilarity in the endmember definition.

3.3.5 Detection of the gap areas

The pre and post-harvest abundance maps were loaded in ENVI version 5.3 using single endmember abundance as gray scale. By plotting the dominant endmember, the gap type is differentiated. If the type is "*Shadowed gap*" then the endmember dominant in the gap area is the shadow endmember. For "*NPV-Soil gap*" the NPV-Soil endmember is the most present. In the case of the "*Understory gap*" the shadow endmember depicts the best the disturbance of the harvest. The vegetation that is exposed after the harvest is not spectrally varying significantly from the vegetation in the pre-harvest dataset. However, the green vegetation remainder in the gap generally belongs to the sub-canopy layers which have lower height than the surrounding main canopy, and then the former gets shadowed by the latter. Therefore, a small increase in the shadow endmember was observed.

Using "*band math*" in ENVI version 5.3, the pre-harvest dataset was subtracted from the post-harvest dataset. This resulted in pixels with high value where the endmember

abundance is increasing and pixels with low value where the endmember abundance is decreasing. After the logging event it was expected to observe an increase in the corresponding endmember in the area where the main tree was removed. The areas that appear with higher value in the endmember abundance difference map should reveal the location that is affected by the logging event. Therefore, the gap is detected by the pixels that showing large change in the endmember difference map. These pixels show a big contrast and this contrast indicates change between the pre and post-harvest datasets and therefore could be used for delineating the affected area.

3.4 Method to derive detectability of the canopy gaps (RQ3)

The last research question is about the spatial resolution requirements of a sensor in order to detect the logging gaps. A detectability analysis was performed for providing the maximum pixel size and the sub-pixel area that should be covered by the gap area in order to be detectable. The steps to answer this question are presented in Figure 10.
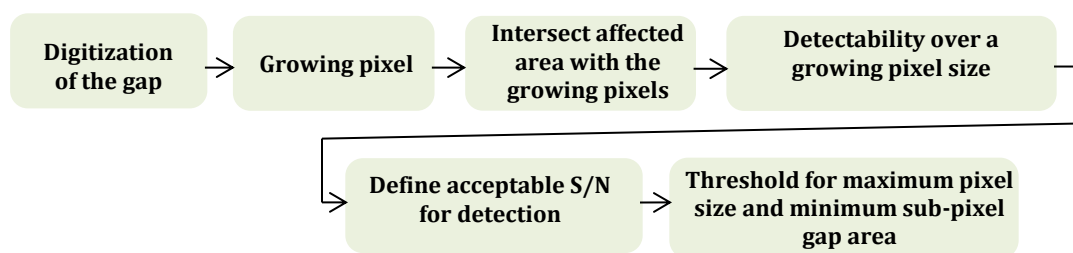
Figure 10. Workflow developed to answer the third research question

3.4.1 Digitization of the affected area

Manual digitization of the gap was used to determine which pixels were included in the affected area. The high value pixels that revealed the logging area were included in the digitizing process. A vector layer was created and then transformed into a Region Of Interest (ROI) providing statistics like the mean value of the endmember difference and the number of the pixels that form the ROI.

3.4.2 Growing Pixel

To analyze the sub-pixel approach, a 1x1 meter pixel was placed manually in the affected area. The pixel was growing by approximately 40x40cm until it reached the borders of the difference dataset. The mean value of each pixel was extracted from the difference dataset. This technique allowed to explore how the endmember difference in the affected area was decreasing as the pixel was growing, including areas where change did not occur. Figure 11 demonstrates how the growing pixel expanded in plot 8 in Guyana. Similarly, the same method used for the other plots.
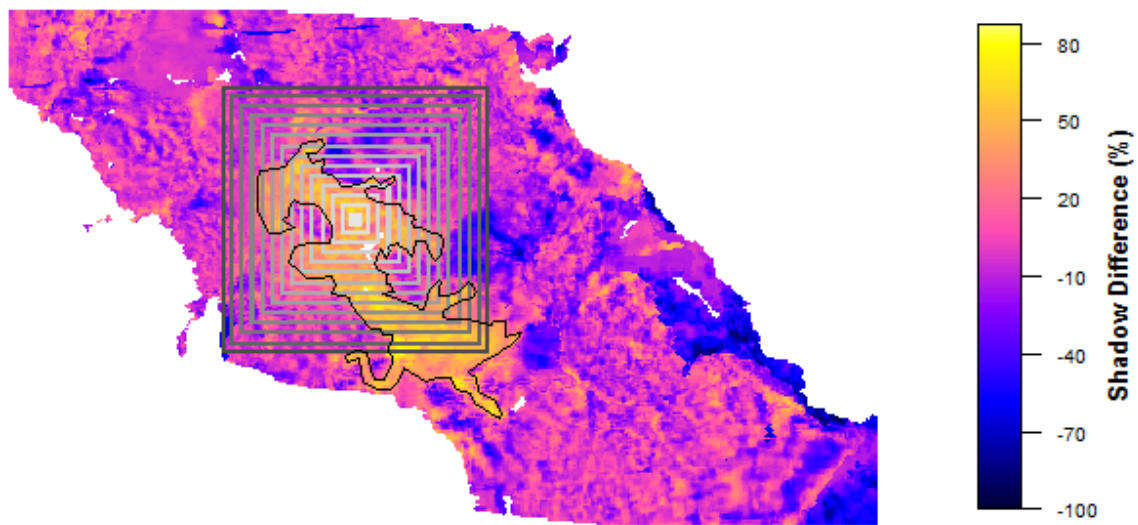
Figure 11. Growing pixel used to extract in this case the mean shadow abundance difference, Guyana plot 8. The black polygon represents the digitized affected area.

3.4.3 Fraction of total pixel area covered by gap area

To find out how much pixel area is covered by gap area, each one of the growing squares was intersected with the gap area. The sub-pixel fraction covered by gap area was calculated dividing the amount of gap pixels by the total amount of pixels for each growing pixel (Figure 12). The gap pixels where calculated intersecting the delineated area with the growing pixel. The number of the intersected pixels was exported to an Excel spreadsheet and the sub-pixel gap area percentage was calculated.
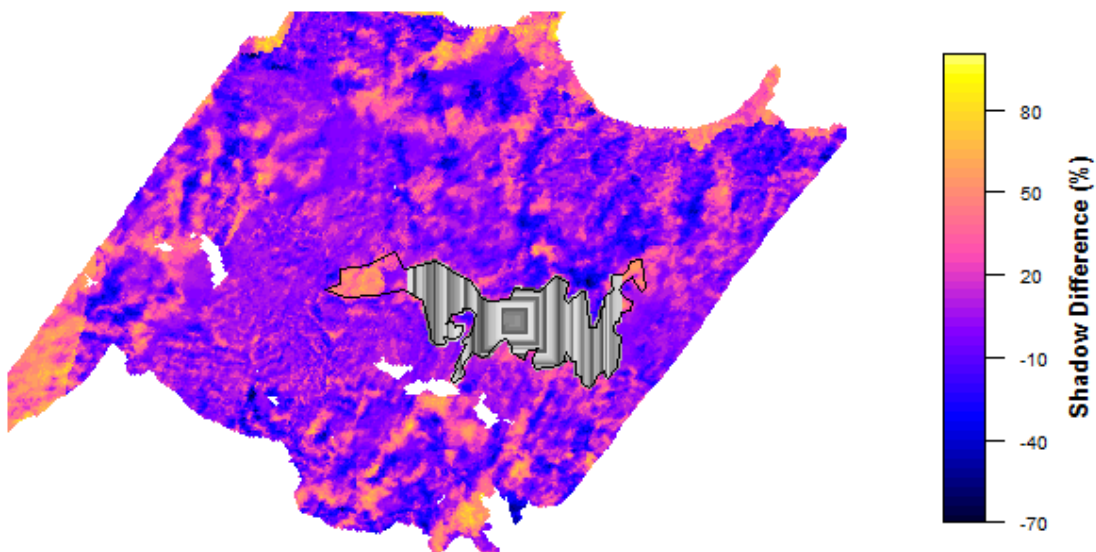
Figure 12. Intersection between the delineated affected area and the growing squares. Guyana plot 6.

3.4.4 Noise quantification

The different illumination (solar angle and viewing conditions) between the two flights and the co-registration inaccuracies introduce incoherency in the pre and post-harvest abundance maps. In the derived abundance maps, changes where the logging did not affect the area can be spotted. This incoherency hereinafter is going to be referred as noise. To quantify the noise, in each plot a sample of 15 circles of around 4 meter radius was taken excluding the area where the logging event affected the canopy (Figure 13).
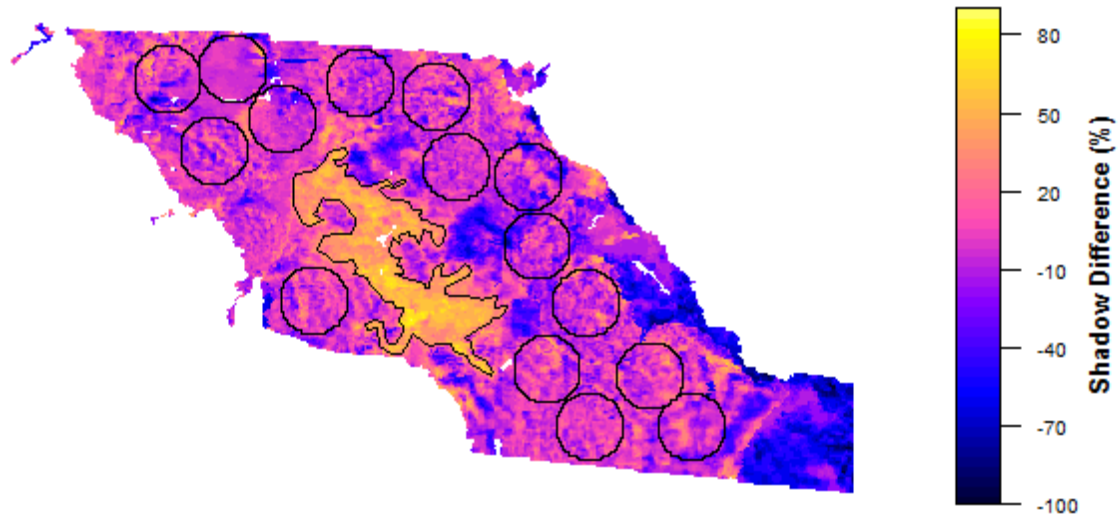
Figure 13. Circles constructed in order to calculate the noise, Guyana plot 8

For the unaffected pixels, it is expected that the endmember fraction should be the same between the pre- and post-harvest datasets. Therefore, the difference between them is indicating the noise level. The mean value of the circles for the corresponding endmember for both pre and post-harvest datasets and their difference was calculated. Below, a detailed explanation of the noise calculation is presented.

The observation can be written mathematically as:

$$SF_{obs} = SF_{real} \pm \sigma_{SF}$$

Where:

SF_{obs} = the measurement

SF_{real} = the noiseless/errorless observation

σ_{SF} = the noise

The noiseless endmember fraction value SFreal is not known and cannot be calculated because there is always some noise in the measurements. What is possible to calculate is a noise estimation. To do that, the first step is to calculate the pre and post-harvest residual for each circle.

$$RES = SF_{post} - SF_{pre}$$

If the method was insensitive to illumination conditions the residual should be always 0. This means that the real value of the residuals is 0 for all the circles. The Root Mean Square Error (RMSE) of the residuals can be calculated and quantify the noise of the residuals.

$$RMSE = \sqrt{\frac{\Sigma(RES)^2}{n}}$$

Where:

n = the number of the observations

$$\sigma_{RES} = RMSE\ (RES,\ 0)$$

Where:

σ_{RES} = Root mean square error of the residuals

To express the relationship between the noise of the residuals and the noise of the observation, error propagation was used.

$$\sigma^2_{RES} = \left(\frac{RES}{SFpre}\right)^2 \sigma^2_{SFpre} + \left(\frac{RES}{SFpost}\right)^2 \sigma^2_{SFpost}$$

The partial derivatives are solved:

$$\frac{RES}{SFpre} = -1, \quad \frac{RES}{SFpost} = 1$$

Assumption that the pre and post observations have the same noise:

$$\sigma_{SF} = \sigma_{SFpre} = \sigma_{SFpost}$$

Making the relation:

$$\sigma^2{}_{RES} = 2\sigma^2{}_{SF}$$

The noise in the endmember abundance observations can be calculated as:

$$\sigma_{SF} = \frac{\sigma RES}{\sqrt{2}}$$

3.4.5 Calculation of Signal to Noise Ratio (SNR)

In this thesis research, signal was defined as the change in endmember abundance between pre and post-harvest datasets where logging occurred. Large abundance difference in the logged area indicates large dissimilarity between the pre and post-harvest datasets hence high signal. Noise is considered as the difference on the pixel values between the two flights in areas where logging did not occur and is calculated as it was described in the section 3.4.4. A signal 10 times greater than the noise was set as the threshold for considering reliable change detection.

3.4.6 Maximum pixel size and minimum sub-pixel gap area

To define the maximum pixel size and the minimum sub-pixel gap area that is detectable for the specific gaps that observed in this research, a threshold of detection is important. This threshold is deriving from the average SNR of each image. This means that the required square (pixel) size will be chosen as the one that includes enough endmember abundance difference (10 times larger than the noise level) to reliably detect the change.

Chapter 4: Results

A Shadowed gap type was created after the selective logging event in all the plots except plot 8 and 11 in Indonesia where an "*Understory gap*" and a "*NPV-Soil gap*" were created respectively.

4.1 Spectral characteristics of forest canopy gaps caused by selective logging (RQ1).

Three types of gaps were distinguished according to their optical properties (spectral signature). Figure 14 presents each gap's spectral signature. The vegetation's spectral signature is included as a reference.

1. The "*Understory gap*" shows a vegetation curve, with chlorophyll absorption at 500 and 650nm and high reflectance in the near-infrared bands.

2. The "*NPV-Soil gap*" shows less absorbance at the 500 and 650nm which indicates less chlorophyll. Moreover, at the near-infrared part of the spectrum their reflectance is not rising as steeply as for the Understory gap signature. However, this increase in the red-edge is indicating the presence of organic matter.

3. The "*Shadowed gap*" reflects the least, representing the dark pixels with a small increase in the near-infrared indicating that the shadowed pixels contain chlorophyll. Moreover, when the light "hits" the vegetation, scatters in multiple directions. The diffuse light which also scatters in the shadowed areas adds to the small increase that can be observed in the near-infrared region.
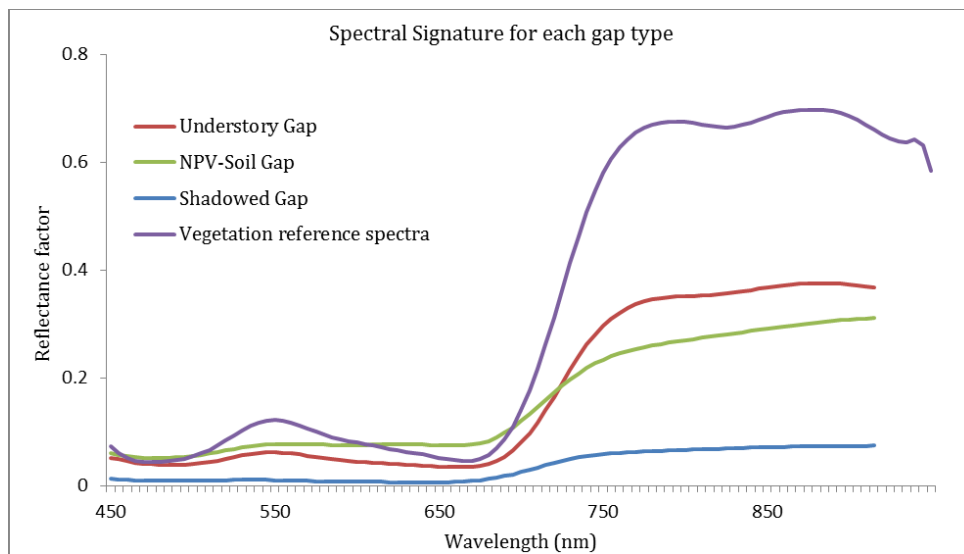
Figure 14. Spectral signature of each gap type. The vegetation spectral signature is provided as reference.

Figure 15 shows how the gap types appear in an RGB photo. These images are taken before and after the harvest of the main tree. The red rectangle represents the delineated plot and the red arrow point to the location where the main tree was harvested. The "*Understory gap*" shows no remarkable difference after the tree removal. When the main tree was removed the secondary vegetation was exposed. This explains why the spectral signature of the "*Understory gap*" is not differentiating much from the green vegetation spectral signature. The "*NPV-Soil gap*" is visibly identifiable as a mixture of NPV, Soil and Green Vegetation (GV). Finally, the "*Shadowed gap*", appears as a dark area where it is not possible to clearly distinguish what is lying beneath the shadow.

Figure 15. RGB photos demonstrating the gap types that can be distinguished in the study areas. A) *"Understory gap"* **in Indonesia plot 8, B)** *"NPV-Soil gap"* **in Indonesia plot 11, and C)** *"Shadowed gap"* **in Indonesia plot 2. In the pre-harvest (left) and post-harvest (right) RGB images the arrows point the location of the main tree (pre) and the affected area (post).**

4.2 Radiometric detection of selectively logged canopy gaps using bi-temporal hyperspectral data (RQ2).

In order to illustrate the use of endmember abundance maps for detection of canopy gaps Figure 16 is provided. The figure depicts the pre- and post-harvest abundance maps for Plot 2 in Indonesia. Each color has 0 as a minimum value and 1 as a maximum. An endmember with high abundance will appear with an intense and clear color. The abundance of each endmember in a pixel is represented by a fraction. In each pixel the sum of all the endmembers will yield 1. The yellow ellipses are placed to point out the location of the logging. In this case, the main tree which was set to fall in northeast direction, took down the neighbor tree also. The logging created a "*Shadowed gap*" as it can be seen in the post-harvest abundance map where an increase in red color is observed. Examining the pre and post-harvest abundance maps it's clear that dissimilarities other than the tree harvest are present. The dissimilarities could be attributed to the differences in viewing conditions and the co-registration process. To avoid repetition, the abundance maps from the rest of the plots are included in Appendix B.
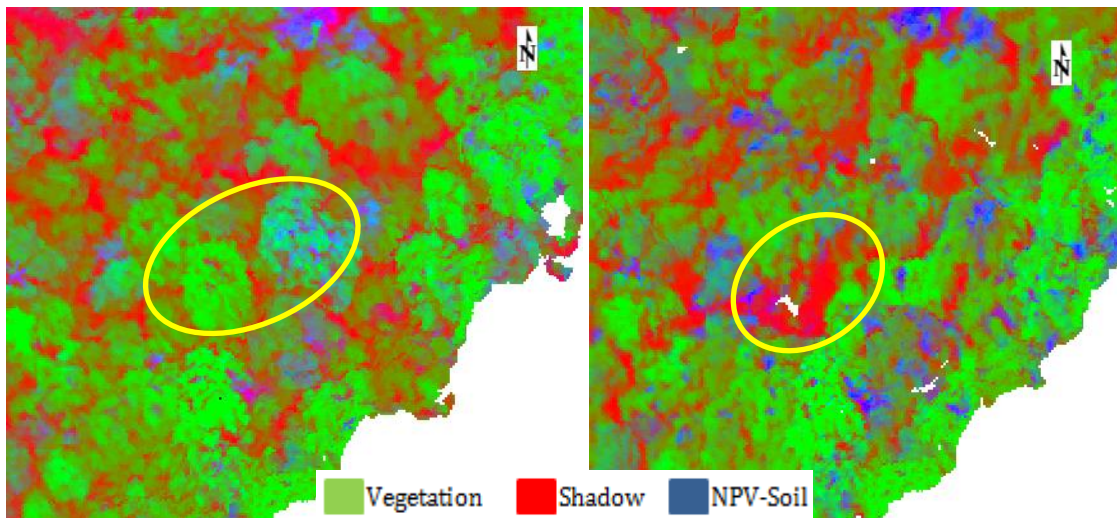
Figure 16. pre (left) and post-harvest (right) abundance maps of Indonesia plot 2. The red color represents the shadow endmember, the green color represents the vegetation endmember and the blue color represents the NPV-Soil endmember. The yellow ellipses indicate the location of the logging.

4.2.1 *"Shadowed gap" detection*

In 5 out of the 7 plots studied a "*Shadowed gap*" type was detected. To illustrate this type of gap detection Figure 17 presents the results of the shadow endmember abundance subtraction for plot 2 in Indonesia. Yellow (increase) and dark blue (decrease) areas indicate change in the endmember abundance in the post-harvest flight. The black polygon specifies the area affected by the logging event. The differences in the endmember abundance where the selective logging did not affect the area are considered as noise. This noise could be attributed to the illumination and viewing conditions (**Error! Reference source not found.**) between the flights, and the co-registration inaccuracies. The large abundance difference around the borders of the datasets can be explained due to the different spatial overlap and the masking that was applied in order to match the borders of the pre and post-harvest datasets. In this plot, after the removal of the main tree, a "*Shadowed gap*" was created. The area that was affected appears with higher pixel values meaning that the shadow abundance was increased. In the other 4 plots where a "*Shadowed gap*" occurred, similar high pixel value areas were detected after the subtraction of the pre and post-harvest shadow abundance maps (Appendix B). The rest of the "*Shadowed gaps*" showed a similar shape. The common characteristic was that the disturbance was creating a gap across the delineated plot, following the direction of the fallen tree.
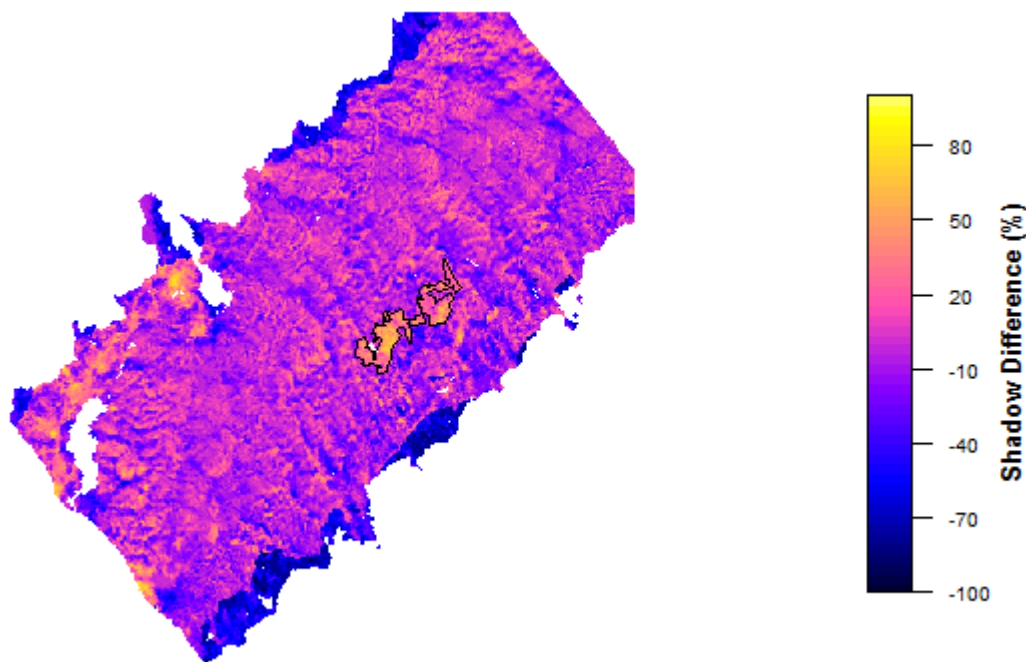
Figure 17. Shadow endmember subtraction between pre- and post-harvest datasets. The black polygon was delineated via the endmember subtraction and indicates the area that was affected after the logging event in Indonesia plot 2

4.2.2 "Understory gap" detection

In plot 8 in Indonesia an "*Understory gap*" was created (Figure 15). In this case, after the tree was harvested the secondary vegetation was exposed. The shadow abundance was increased also, but the increase was subtle. Still, the shadow abundance difference is pointing out the affected area. The difference is small because as the tree was falling it did not destroy the surrounding canopy vegetation but rather expose it. To detect that subtle change, a prior knowledge of the logged area was of great assistance. Radiometrically there is a very small difference in the logged area's averaged spectral characteristics (Figure 18). This figure shows the delineated affected area which was derived by the subtraction of the two shadow endmember abundance maps and how the average spectral signature reacts to the change. It appears that the logged area reflects more in the NIR part of the spectrum before the harvest of the main tree.
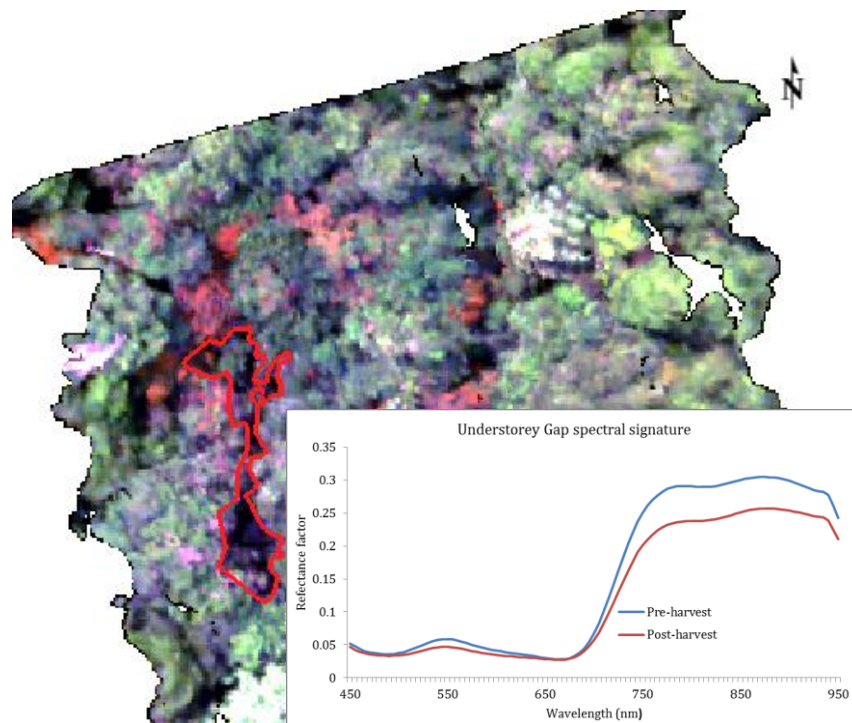
Figure 18. pre and post-harvest spectral signature of the logged area. The affected area is indicated by the red polygon. The wavelengths chosen for the RGB visualization is 665nm (red), 565nm (green), and 465nm (blue).

Subtracting the shadow abundance datasets revealed a small increase in shadow abundance after the logging event (Figure 19). The shadow abundance increase which in this case is

subtle shows that the "Understory gap" is similar to the "Shadowed gap" in terms of shadow increase. However, the "Understory gap" exposes vegetation and therefore the shadow increase is considerably less than the increase that has been visually detected in the "Shadowed gap" RGB image (Figure 15)Figure 15. RGB photos demonstrating the gap types that can be distinguished in the study areas. A) "*Understory gap*" in Indonesia plot 8, B) "*NPV-Soil gap*" in Indonesia plot 11, and C) "*Shadowed gap*" in Indonesia plot 2. In the pre-harvest (left) and post-harvest (right) RGB images the arrows point the location of the main tree (pre) and the affected area (post). This result agrees with Figure 18 which shows the pre-logged area to reflect more than the post-logged area.
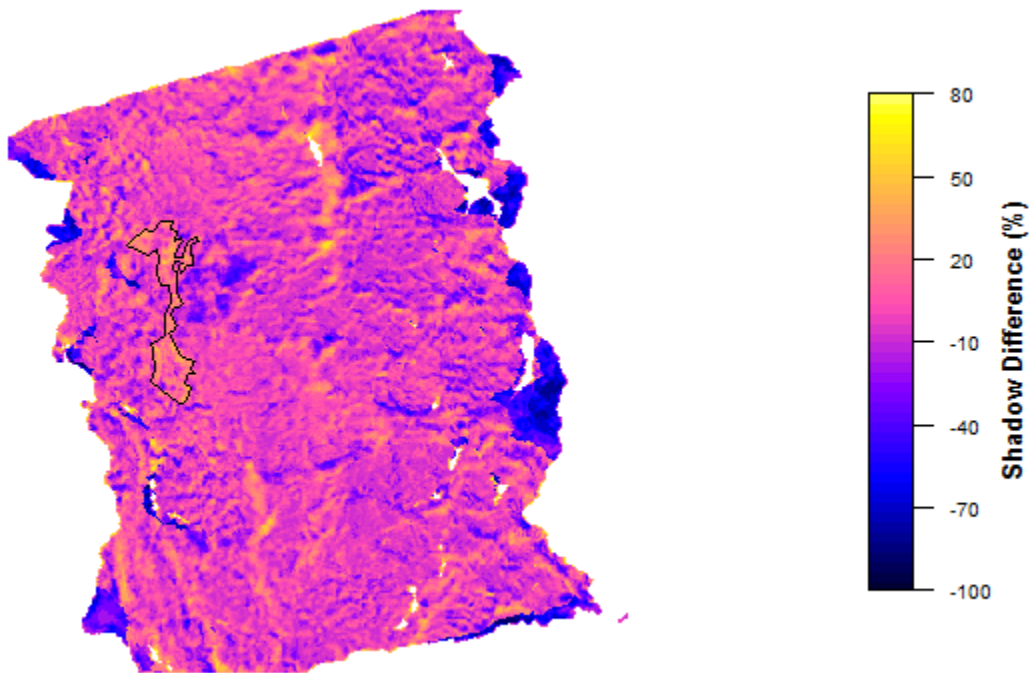
Figure 19. Shadow endmember subtraction dataset. The black polygon indicates the area that was affected after the logging event in Indonesia plot 8.

4.2.3 "NPV-Soil gap" detection

In plot 11 in Indonesia an "*NPV-Soil gap*" the NPV-Soil endmember was used for the subtraction. In Figure 20 the subtraction between the pre and post-harvest abundance maps is presented. Like the previous gap types, the affected area appears bright. The pixels with high value indicate the location where the NPV-Soil endmember increased after the logging event. The black polygon delineates the area that the tree landed creating an "*NPV-Soil gap*".
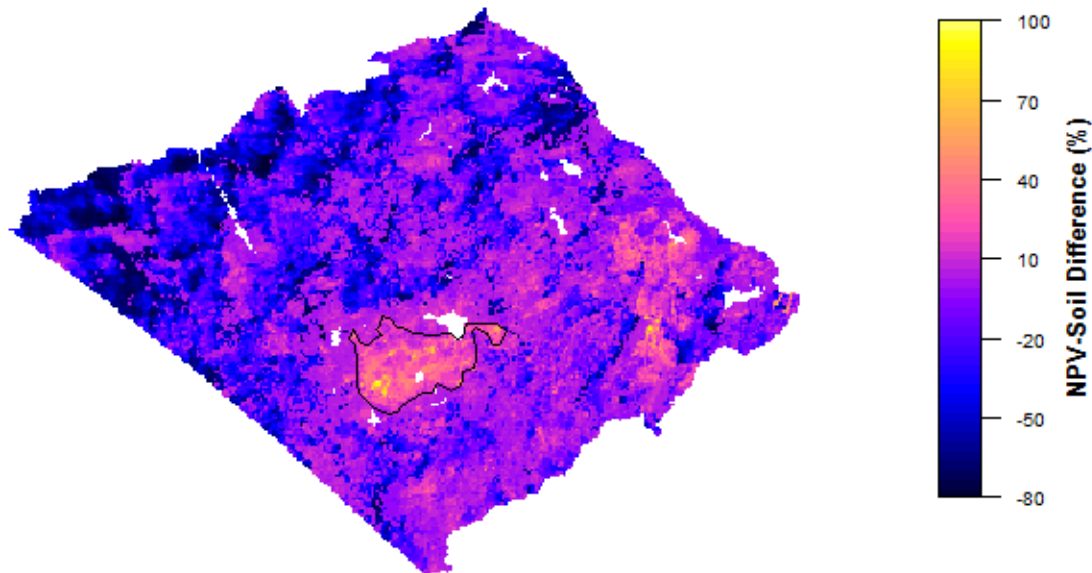
Figure 20. NPV-Soil endmember subtraction dataset. The black polygon indicate the area that was affected after the logging event in Indonesia plot 11.

4.3 How big should the pixel size be and how much sub-pixel area should the gap cover in order to detect it (RQ3)?

Following the steps described in the methodology chapter, the relationship between the endmember fraction difference and the sub-pixel area that the gap covers is illustrated in Figure 21. This figure includes all the plots where a gap was created after the tree harvest. It can be seen that as the sub-pixel gap cover is decreasing, the difference in the endmember abundance is also decreasing. This happens because the pixel encloses areas without change (except noise) meaning that the difference in the endmember abundance is fading.
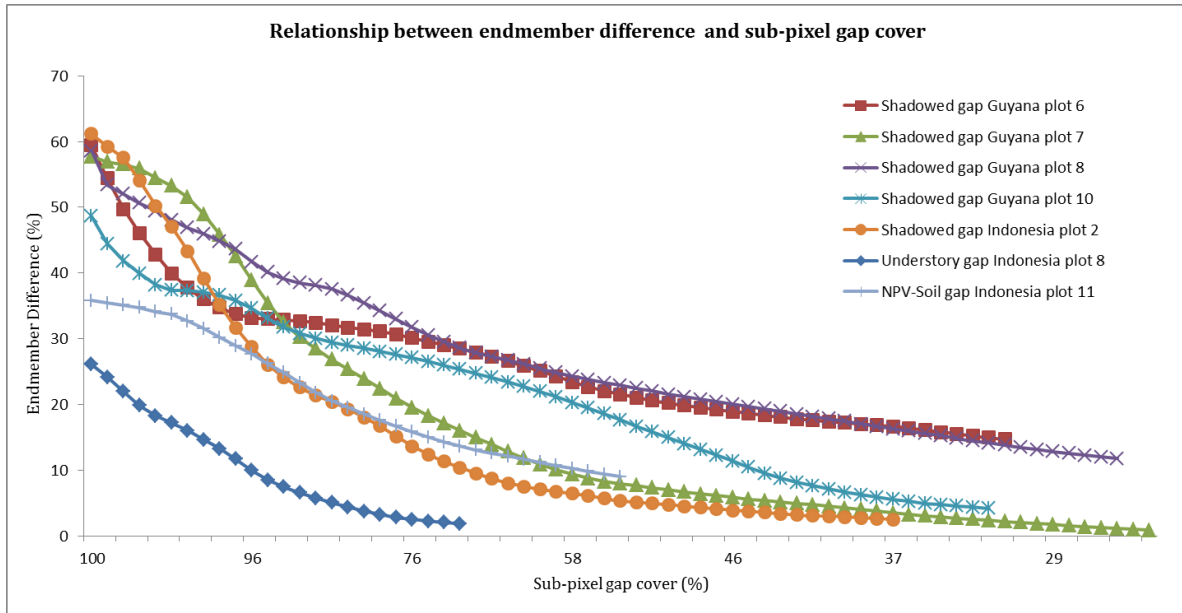
Figure 21. Graph demonstrating how the detectability of the each gap is decreasing as the sub-pixel gap cover is decreasing

Figure 22 shows how big the pixel should be in order to reliably detect a shadowed gap. The noise was averaged using all the plots available (7). The Δ-shadow-abundance values were averaged over the 5 plots values in order to combine the information of the different plots where a *"Shadowed gap"* was created. The average noise was calculated to 2.56% ranging from 0.9-4.6%. The averaged noise gives an indication about the signal needed for reliable detection. As it was stated in the methodology chapter, a SNR ten times greater than the noise was set as reliable detection. This means 25.6% of endmember abundance difference is the threshold for a reliable detection. This threshold translates in at least a 9.3x9.3 m² pixel size in order to detect shadowed gaps. However, in Figure 22 the upper and lower limits (black dotted lines) show that the 9.3x9.3 m² pixel size cannot be used to detect all 5 *"Shadowed gaps"*. The range of the limits is between 6x6 m² and 13.3x13.3 m² pixel sizes.
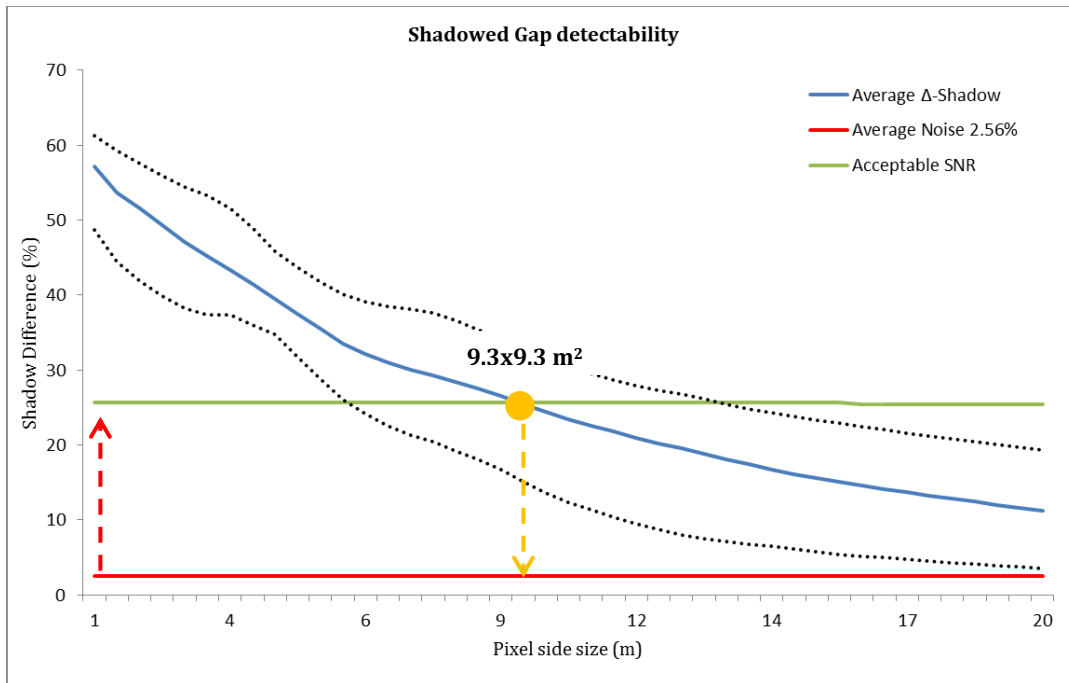
Figure 22. Relationship between averaged Δ-Shadow and pixel size (blue line). The dotted black lines represent the max and min values of the averaged Δ-Shadow curve. The X axis value corresponding to the intersection (orange dot) between the green line (acceptable signal for reliable detection) and blue line provides the required pixel size for reliable shadowed gap detection.

4.3.1 NPV-Soil Gap

This type of gap occurred in plot 11 in Indonesia where after the removal of the valuable tree, an area with Soil-NPV and Vegetation in the form of broken leafed branches was created (Figure 23).

Figure 23. Indonesia plot 11, Soil-NPV gap indicated by the red ellipse. RGB photo from the post-harvest UAV flight

Like the shadowed gap, the "*NPV-Soil gap*" in Indonesia plot 11 shows similar behavior when the NPV-Soil difference is plotted against the pixel size (Figure 24). As the pixel size is growing, the difference is decreasing. Applying the same average noise level (2.56%) and the reliable SNR (x10) provided an acceptable signal (endmember abundance difference) of 25.6%, and therefore the required pixel size for a reliable detection is equal or larger than 7x7 m².
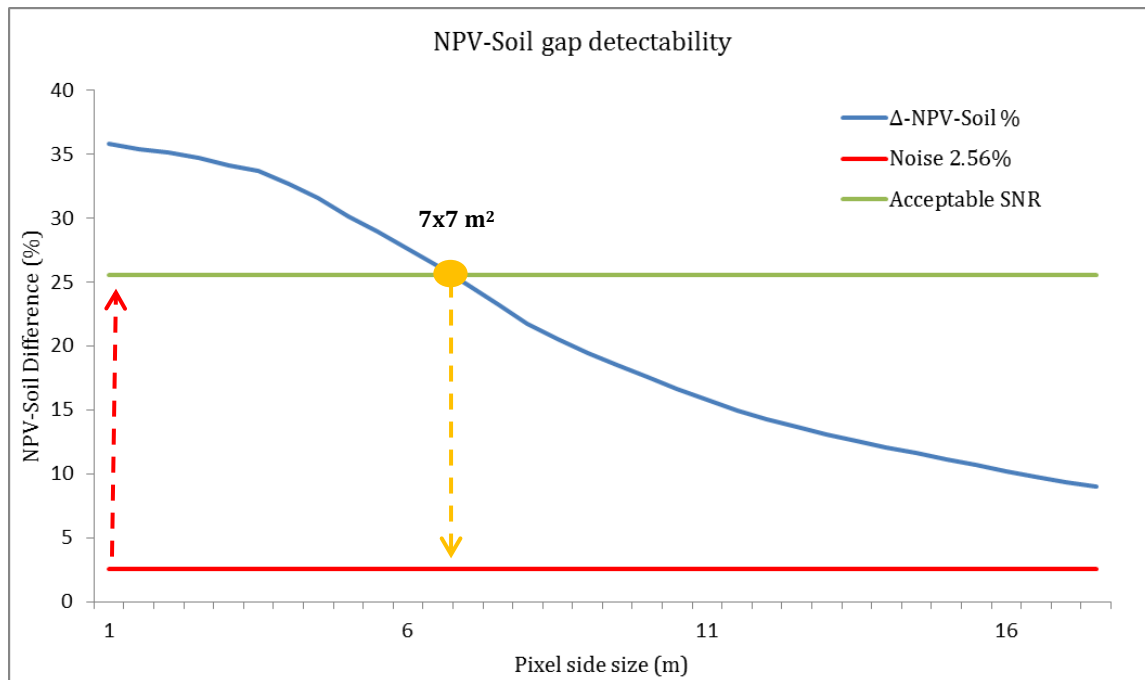
Figure 24. Relationship between Δ-NPV-Soil and pixel size. The intersection between the green and blue line represent the required pixel size for NPV-Soil gap detection

4.3.2 Understory Gap

Figure 25 shows the relationship between the shadow abundance difference and the pixel size for the plot with an Understory gap type (Indonesia Plot 8). Similarly with the other gap types, as the sampling pixel is growing the shadow abundance difference is decreasing (including more unaffected pixels). Applying the acceptable SNR and using averaged noise, the threshold of reliable detection was set at 25.6%. This translates to a pixel size of 1x1 m². This is the smallest required pixel for detection across the three gap types. This is happening because the disturbance was very subtle. Almost did not exceed the detection threshold.
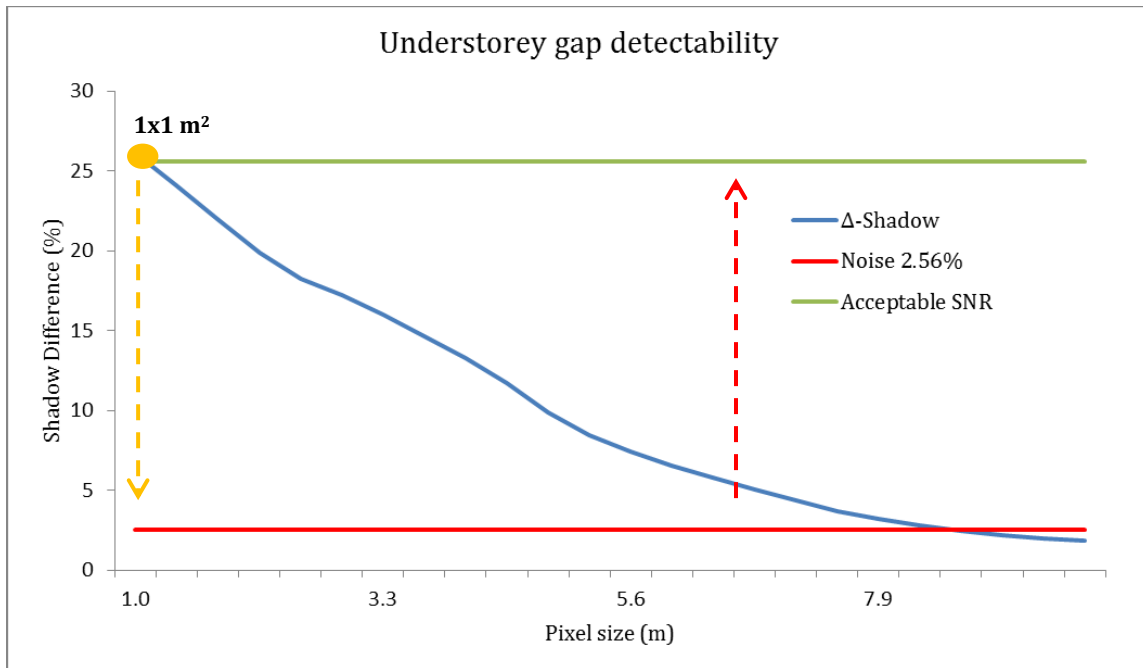
Figure 25. Relationship between shadow difference and pixel size. The intersection between the green and blue line represent the required pixel size for detection

4.3.3 Overview

Table 3 gives an overview of the results of research question 3. The table includes the sub-pixel area (%) that a gap should cover in order to be detectable, the corresponding pixel size (m^2) and the average noise (%).

In the plots that contained a shadowed gap, the gap size is averaged to 189 m^2. The averaged sub-pixel area that the gap covered was 68% and the corresponding pixel size for reliable detection was 9.3x9.3 m^2. As it was stated in section 4.3 this pixel size might not be able to detect all the "*Shadowed gaps*". This size is calculated by averaging 5 plots, with a lower limit of 6x6 m^2 and an upper limit of 13.3x13.3 m^2 pixel sizes.

The NPV-Soil gap size was 79 m^2. And the sub-pixel area that should be covered by gap area in order to be detected was 89% of the pixel which in this case corresponds to a pixel's size of 7x7 m^2.

Finally, the "Understory gap" was the smallest with a size of 51 m^2. This gap affected the less the neighbor vegetated areas resulting into the very high spatial resolution pixel size requirement of 1x1 m^2 in order to be detected. Moreover, the pixel has to contain 100% of gap area to be detected.

Table 3. Overview of the results for each gap type

Gap Type	Plot	Average Gap Size (m²)	Maximum Pixel Size (m²)	Average Sub-pixel gap area (%)	Average Noise (%)
Shadow	Indonesia 2 Guyana 6 Guyana 7 Guyana 8 Guyana 10	189	9.3x9.3	68	2.56
NPV-Soil	Indonesia 11	79	7x7	89	
Understory	Indonesia 8	51	1x1	100	

Chapter 5: Discussion & Conclusions

5.1 Discussion

5.1.1 Spectral properties of canopy gaps, RQ1

It is important to distinguish the gaps according to their spectral properties because if one is only looking to detect "*NPV-Soil gaps*" the results will underestimate the selective logging activity in the area. "*Shadowed gap*" or "*Understory gap*" type is a possibility when selective logging occurs. However, the gap types are strongly connected with the solar illumination angle and the gap's structural characteristics (size, shape and height of remaining vegetation in relation to the surrounding canopy height). The solar angle causes certain areas to be illuminated or shaded (Koukoulas and Blackburn 2004). For example, an "*NPV-Soil gap*" at 12:00 p.m. could be transformed in a "*Shadowed gap*" at 16:00 p.m. this means that the gaps that were studied in the scope of this research could reflect completely different if the images were acquired in different time of the day. This is not a problem for satellites that will acquire imagery always at the same time of the day. Nevertheless, integrating data between satellites that are not synchronized would be problematic. Moreover, due to the fast regrowth in the tropics an "*NPV-Soil gap*" could very fast be vegetated resulting in the decrease of the spectral difference (Miettinen et al., 2014) which is important in order to detect change when comparing data acquired in different instances. However, the cloudy atmospheric conditions that are very common in the tropical regions make the cloudless image acquisition very hard.

5.1.2 Spectral unmixing for gap detection, RQ2

The main issue with the detection of selective logging in other studies (Stone & Lefebvre 1998, Asner et al., 2004 and Negron-Juarez et al. 2011) was the small scale of the logging

disturbance. In those studies, the disturbance was smaller than the pixel size and therefore a robust detection was not feasible. To counter this problem, sensors with higher spatial resolution and spectral unmixing analysis were used (Franke et al., 2012). In this thesis research the pixel size was not an issue, using a hyperspectral dataset with the spatial resolution to range in centimeters. Applying the SMACC spectral unmixing algorithm it was possible to derive abundance maps for the defined endmembers and detect the logged area. The endmembers were defined keeping in mind that the study areas consist of pure forest without man-made objects and therefore the endmembers would relate to expected spectral properties. Out of the three defined gap types (*Shadow*, *NPV-Soil* and *Understory*) the "*Understory gap*" was the most difficult to detect due to the low spectral difference between the pre- and post-harvest datasets. The low spectral difference can be attributed to the understory vegetation that was exposed after the selective logging. The understory vegetation does not provide a large spectral difference between the pre- and post-harvest datasets as the "*Shadowed*" and "*NPV-Soil gap*" types do. A small increase in the shadow abundance was the indication that there was a disturbance in the area. However, for all the gap types the noise that was introduced to the difference maps through the different illumination conditions (solar angle, viewing conditions) and the co-registration inaccuracies made the detection trickier as areas other than the logged ones would be wrongly detected as areas that change occurred. The noise could be reduced using a satellite that will fly over the same area at the same time eliminating the solar angle difference. Nevertheless, the spatial resolution should be high enough to detect the small scale selective logging. A limitation that the optical sensors cannot counter is the cloudy atmospheric conditions in the tropics (Mietinen et al., 2014). Even with a UAV that flies under the clouds, the shadowing effect that is introduced by the clouds cannot be eliminated. The cloudy conditions in combination with the fast regrowth of the logged areas are the reason why a dense multi-temporal image acquisition for monitoring the tropics is of great importance.

5.1.3 Detectability analysis, RQ3

The detectability analysis showed that in order to detect selective logging using the difference of abundance maps, the pixel must contain a large part of the gap (Table 3). Taking into consideration the small scale of selective logging events, this implies that very-high resolution sensors are needed in order a big part of the changed area will be included by the pixel. Table 3 shows that the averaged pixel size to detect a shadowed gap is 9.3x9.3 m^2 and the area that should be covered by the gap is 68%. However, these values are calculated averaging the size of the *"Shadowed gaps"* indicating that not all the "*Shadowed gaps*" will be detected by this pixel size. Moreover, to test the detectability, the center of the growing pixel was placed where the pixels appeared with higher value in the difference maps. In reality, the pixel is placed automatically according to the sensor's technical characteristics. The issue that rises over that acknowledgement is that the 9.3x9.3 m^2 will not derive the same results if the pixel will be placed in a slightly different position than the one tested in this research because the sub-pixel gap area cover will be lower. This means that the sub-pixel gap area might not be enough for detection for the proposed pixel size. Figure 26 gives an example of the random pixel placement issue. In the image that the pixels placed randomly (right), the sub-pixel gap area cover is smaller than the one with the manual placement (left). In this case the gap in the left image will be detected but in the right will not. The black pixel in Figure 26 indicates that the gap should cover a larger sub-pixel area.
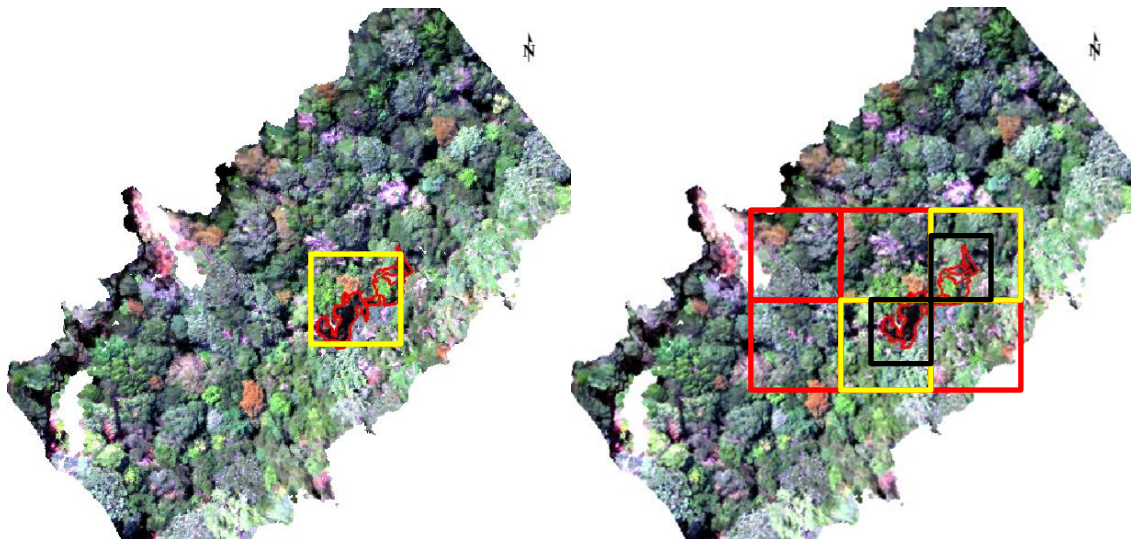
Figure 26. Example of the random placement issue. In the left image the pixel was placed manually and is including a big part of the gap. In the right image the pixels were placed randomly resulting in smaller sub-pixel gap area coverage. The yellow pixels in the right image demonstrate that if the 9.3x9.3 m^2 is placed randomly it might not include enough gap area for detection. The black pixels indicate that in real life situations smaller pixel size than those in Table 3 are needed because in random placement the pixel might not include enough gap area for detection.

Franke et al., 2012 used RapidEye MSI to apply MTMF, a spectral unmixing algorithm to detect illegal selective logging. They stated that spaceborne sensors like QuickBird-2, WorldView2, SPOT-5 HRG, RapidEye MSI, GeoEye-1, IKONOS-2 MS, THEOS MS could in principle be used to monitor small scale forest disturbances due to their very-high spatial and temporal resolution. The proposed satellite sensors are ranging from 1.5m – 15m in spatial resolution. However the aforementioned research considered NPV and Soil as the only spectral signatures that indicates selective logging.

5.2 Conclusions

Small scale selective logging in the studied area created gaps with different spectral properties. This spectral variation should be taken into consideration when looking to detect selectively logged areas. Gaps other than "*NPV-Soil*" type can be created after small scale selective logging resulting in underestimation of the areas that are affected by selective logging. The gaps were categorized into three types according to their spectral properties. The "*Shadowed gap*", the "*NPV-Soil gap*" and the "*Understory gap*".

Using high spatial and spectral resolution hyperspectral data it was possible to apply spectral unmixing using the SMACC algorithm and derive abundance maps for each endmember. Through a subtraction of the corresponding endmember (type of gap) for pre and post-harvest datasets it was feasible to detect areas that changed due to a selective logging event. In some occasions like the "Understory gap", it was very hard to spot the gap. Noisy areas were also appearing with high value pixels making the detection uncertain. However, the RGB and DSM datasets were of great help to spot the changes.

The detectability analysis showed that the detectability of the selective logging depends on many factors. The noise level is an important one defining the minimum detectable disturbance. Also the gap size, shape and other structural characteristics is relevant to the required pixel size. This indicates that as the gap size is growing, bigger pixels are suitable for detection. However, the detectability analysis showed that the gap area should cover at least 68% of the pixel area in order to be detected. This coverage percentage in combination with the observed small gap sizes, indicate that the pixel size should be small enough in order to include a big part of the gap. This leads to the conclusion that even with the SMACC sub-pixel approach; the gap area should cover a very big part of the pixel in order to be detected.

This research showed that a typical "Shadowed gap" size (averaged from 5 plots) is 189 m^2. This corresponds to a minimum of 68% sub pixel gap coverage and a maximum of 9.3x9.3 m^2 pixel size requirement for detection. However these requirements are not representative for all the "Shadowed gaps" but only for the averaged "Shadowed gap" size. The "NPV-Soil gap" size was 79 m^2 which corresponds to 89% minimum sub-pixel gap area and a 7x7 m^2 maximum pixel size requirement for detection. Lastly, the "Understory gap" size was 51 m^2 which corresponds to a full (100%) gap coverage by a 1x1 m^2 pixel.

Due to the pixel random placement issue, smaller pixel sizes than 9.3x9.3 m^2, 7x7 m^2 and 1x1 m^2 (depending on the gap type) are required in order to detect the gaps in this study. The detectability analysis showed that the "*NPV-Soil gap*" and "Shadowed gaps" could be detected using bigger pixels than the "*Understory gap*" where the pixel size should be much smaller. However the detection is very closely connected to the gap's size. Even an "Understory gap" could be detected with a coarser spatial resolution if its size was big enough. More gap samples are needed in order to define a decisive pixel size for detection. Especially for the "*NPV-Soil gap*" and "*Understory gap*" types where only one sample was considered. However an indication of the gap sizes and types that one can meet in the tropics has been given alongside with the difficulties and the limitations of the small scale selective logging detection in the tropics.

References

Asner, G. P., M. Keller, R. Pereira Jr., and J. C. Zweede. 2002a. Remote sensing of selective logging in amazonia: Assesing limitations based on detailed field observations, Landsat ETM+, and textural analysis. Remote Sens. Environ. 80: 483-496.

Asner, G. P., M. Palace, M. Keller, R. Pereira Jr., J. N. M. Silva, and J. C. Zweede. 2002b. Estimating Canopy Structure in an Amazon Forest from Laser Range Finder and IKONOS Satellite Observations. Biotropica 34: 483-492. doi:10.1111/j.1744-7429.2002.tb00568.x.

Asner, G. P., M. Keller, R. Pereira Jr., J. C. Zweede, and J. N. M. Silva. 2004. Canopy Damage and Recovery after Selective Logging in Amazonia: Field and Satellite Studies. Ecological Applications 14: 280–298. doi:10.1890/01-6019.

Brokaw, N. V. L., 1982. The definition of treefall gap and its effect on measures of forest dynamics. Biotropica, 14, 2, 158-160.

Brokaw, N., and J. Grear. 1991. Forest Structure Before and After Hurricane Hugo at Three Elevations in the Luquillo Mountains, Puerto Rico. Biotropica 23: 386–392. doi:10.2307/2388256.

Dubayah, R. O., and J. B. Drake. 2000. Lidar Remote Sensing for Forestry Applications. Journal of Forestry 98: 44–46.

FAO, 2010a. Global forest resources assessment 2010: terms and definitions. FAO working paper 144/E. Food and Agriculture organization (FAO) of the United Nations (UN), Rome.

FAO, 2011a. Assessing forest degradation, Towards the development of globally applicable guidelines, Working Paper 177.

FAO, 2011b. Southeast Asian forests and forestry to 2020, Subregional report of the second Asia-Pacific forestry sector outlook study. Food and Agriculture Organization (FAO) of the United Nations (UN), Regional office for Asia and the Pacific, Bangkok.

Ferrazoli, P., and L. Guerriero. 1994. Interpretation and Model Analysis of Maestro 1 Flevoland Data. International Journal of Remote Sensing 15: 2901–2915. doi:10.1080/01431169408954291.

Gong, P., G. S. Biging, and R. Standiford. 2000. Use of Digital Surface Model for Hardwood Rangeland Monitoring. Journal of Range Management 53: 622–626.

Green, K. 2000. Selecting and Interpreting High Resolution Images. Journal of Forestry 98: 37–39.

Gruninger, J., Ratkowski, A. J., & Hoke, M. L. 2004. The sequential maximum angle convex cone (SMACC) endmember model. Paper presented at the Proceedings of SPIE - The International Society for Optical Engineering.

Harding, D. J., M. A. Lefsky, G. G. Parker, and J. B. Blair. 2001. Laser Altimeter Canopy Height Profiles: Methods and Validation for Closed-Canopy, Broadleaf Forests. Remote Sensing of Environment 76: 283–297. doi:10.1016/S0034-4257(00)00210-8.

Herold, M., Skutch, M., 2011. Monitoring, reporting and verification for national REDD+ programmes: two proposals. Environmental Research Letters 6, http://dx.doi.org/10.1088/1748-9326/6/1/014002.

Imhoff, M. L. 1995. A Theoretical Analysis of the Effect of Forest Structure on Synthetic Aperture Radar Backscatter and the Remote Sensing of Biomass. IEEE Transactions on Geoscience and Remote Sensing 33: 341–352. doi:10.1109/36.377934.

Kissinger, G., Herold, M., De Sy, V., 2012. Drivers of deforestation and forest degradation: a synthesis report for REDD+ policymakers. Lexeme Consulting, Vancouver, Canada.

Koukoulas, S., & Blackburn, G. A., 2004. Quantifying the spatial properties of forest canopy gaps using LiDAR imagery and GIS. International Journal of Remote Sensing, 25(15), 3049-3071. doi: 10.1080/01431160310001657786

Malahlela, O., Cho, M. A., & Mutanga, O., 2014. Mapping canopy gaps in an indigenous subtropical coastal forest using high-resolution WorldView-2 data. International Journal of Remote Sensing, 35(17), 6397-6417. doi: 10.1080/01431161.2014.954061

Miettinen, J., Stibig, H. J., & Achard, F., 2014. Remote sensing of forest degradation in Southeast Asia-Aiming for a regional view through 5-30 m satellite data. Global Ecology and Conservation, 2, 24-36. doi: 10.1016/j.gecco.2014.07.007

Mon, M. S., Mizoue, N., Htun, N. Z., Kajisa, T., & Yoshida, S. 2012. Factors affecting deforestation and forest degradation in selectively logged production forest: A case study in Myanmar. Forest Ecology and Management, 267, 190-198. doi: 10.1016/j.foreco.2011.11.036

Mutanga, O., E. Adam, and M. A. Cho. 2012. High Density Biomass Estimation for Wetland Vegetation Using Worldview-2 Imagery and Random Forest Regression Algorithm. International Journal of Applied Earth Observation and Geoinformation 18: 399–406. doi:10.1016/j.jag.2012.03.012.

Negron-Juarez, R.I., Chambers, J.Q., Marra, D.M., Ribeiro, G.H.P.M., Rifai, S.W., Higuchi, N., Roberts, D., 2011. Detection of subpixel treefall gaps with landsat imagery in Central Amazon forests. Remote Sens. Environ. 115, 3322–3328.

Nelson, R., R. Oderwald, and T. G. Gregoire. 1997. Separating the Ground and Airborne Laser Sampling Phases to Estimate Tropical Forest Basal Area, Volume, and Biomass. Remote Sensing of Environment 60: 311–326. doi:10.1016/S0034-4257(96)00213-1.

Nurhayati, R., 2015. Individual tree crown delineation in tropical forest using object-based analysis of orthoimage and digital surface model. Laboratory of Geo-Information Science and Remote Sensing, Thesis Report GIRS-2015-35, Wageningen University.

Oldeman, R. A. A., 1978. Architecture and energy exchange of dicotyledonous trees in the forest. In: Tomlinson P. B. & Zimmerman M. H., eds., Tropical trees as living systems, Cambridge University Press, Cambridge, U.K., 535-560.

Pithon, S., Jubelin, G., Guitet, S., Gond, V., 2013. A statistical method for detecting logging-related canopy gaps using high-resolution optical remote sensing. Int. J. Remote Sens. 34, 700–711.

Popma, J., Bingers F., Martinez-Ramos M. & Veneklaas E., 1988. Pioneer species distribution in treefall gaps in Neotropical rain forest; a gap definition and its consequences. Journal of Tropical Ecology, 4, 77-78.

Romijn, E., Ainembabazi, J. H., Wijaya, A., Herold, M., Angelsen, A., Verchot, L., & Murdiyarso, D. 2013. Exploring different forest definitions and their impact on developing REDD+ reference emission levels: A case study for Indonesia. Environmental Science and Policy, 33, 246-259. doi: 10.1016/j.envsci.2013.06.002

Runkle, J. R. 1981. Gap regeneration in some old-growth forests of the eastern United States. Ecology, 62, 4, 1041-1051.

Runkle, J. R. 1982. Patterns of Disturbance in Some Old-Growth Mesic Forests of Eastern North-America. Ecology 63: 1533–1546. doi:10.2307/1938878.

Schlich, W., 1907. Sir Dietrich Brandis, K.C.I.E., F.R.S.. Nature 76, 131-132.

Souza Jr., C., Roberts, D.A., Cochrane, M.A., 2005. Combining spectral and spatial information to map canopy damage from selective logging and forest fires. Remote Sens. Environ. 98, 329–343.

Stibig, H.-J., Stolle, F., Dennis, R., Feldkötter, C., 2007b. Forest Cover Change in Southeast Asia-The Regional Pattern. EUR-Scientific and Technical Research Series. EUR 22896 EN. Office for Official Publications of the European Communities, Luxembourg, p.41.

Stone, T. A., & Lefebvre, P. (1998). Using multi-temporal satellite data to evaluate selective logging in Para, Brazil. International Journal of Remote Sensing, 19, 2517– 2526.

Suomalainen1, Juha, Niels Anders, Shahzad Iqbal, Gerbert Roerink, Jappe Franke, Philip Wenting, Dirk Hünniger, Harm Bartholomeus, Rolf Becker, and Lammert Kooistra. 2014. "A Lightweight Hyperspectral Mapping System and Photogrammetric Processing Chain for Unmanned Aerial Vehicles." Remote Sensing 6: 1–26. doi:10.3390/rs60x000x.

Swellengrebel, E. J. G. 1959. On the Value of Large-Scale Aerial Photographs in British Guiana Forestry. Empire Forestry Review 38: 54–64.

Ter Steege, H., Welch, I., Zagt, R., 2002. Long-term effect of timber harvesting in the Bartica Triangle, Central Guyana. For. Ecol. Manage. 170, 127-144. doi: 10.1016/S0378-1127(01)00777-0

Whitmore, T. C., Brown N. D., Swaine M. D., Kennedy D., Goodwin-Bailey C. I. & Gong W. K., 1993. Use of hemispherical photographs in forest ecology: measurement of gap size and radiation totals in a Bornean tropical rain forest. Journal of Tropical Ecology, 9, 131-151.

Wilcove, D.S., Giam, X., Edwards, D.P., Fisher, B., Koh, L.P., 2013. Navjot's nightmare revisited: logging, agriculture, and biodiversity in Southeast Asia. Trends Ecol. Evolut. 28, 531–540.

Woodcock, C. E., S. A. Macomber, M. Pax-Lenney, and W. C. Cohen. 2001. Monitoring Large Areas for Forest Change Using Landsat: Generalization across Space, Time and Landsat Sensors. Remote Sensing of Environment 78: 194–203. doi:10.1016/S0034-4257(01)00259-0.

Appendices

Appendix A: R script to align the pre- and post-harvest datasets

library (raster) #Install raster library

library (rgdal) #Install rgdal library

setwd ("C:/Guyana10/Original") #set working directory to the correct folder

list.files() #Print the data names contained in the folder

x.1<-
brick("Pre_HyperspectralDatacube_FlightLine01_PixelSize=0.227m_DSM=Photogram metric_FWHM=30nm.bsq") #load the pre-harvest dataset as raster brick

setwd("C:/Guyana10/Warped")

list.files()

x.2 <- brick("Post_G10_Warped.dat") #load the post-harvest warped dataset as raster brick

x.i <- intersect(extent(x.1), extent(x.2)) # find intersection of the pre- and post-harvest extent

r.i <- crop(x.1, x.i) # create intersect raster with required dimensions

x.1.s <- crop(x.1, extent(r.i)) #crop pre-harvest dataset using the extent of the intersected raster

extent(x.1.s) <- alignExtent(x.1.s, r.i) #align the two rasters

#same process for the post-harvest dataset

x.2.s <- crop(x.2, extent(r.i))

extent(x.2.s) <- alignExtent(x.2.s, r.i)

x.2.s[is.na(x.2.s)] <- 0

setwd("C:/Guyana10/Rallign")

#export rasters in GTiFF format

writeRaster(x.1.s,filename = "Pre10.tif",format = "GTiff")

writeRaster(x.2.s,filename = "Post10NONA.tif",format = "GTiff")

Appendix B: Abundance Maps

This appendix includes the abundance maps as they were derived by the SMACC algorithm. Each color represents high endmember abundance. The scale of each endmember is ranging from 0 to 1. The shadow endmember is corresponding to green color, the vegetation endmember to red color and endmember 3 to blue color. Endmember 3, in Guyanese plots represent vegetation whereas in Indonesian plots represents a mixture of NPV and Soil.

A)

Vegetation   Shadow   NPV-Soil

B)

Vegetation   Shadow   NPV-Soil

C)

Vegetation Shadow NPV-Soil

D)

Vegetation Shadow Endmember 3

E)

F)

G)

Vegetation   Shadow   Endmember 3
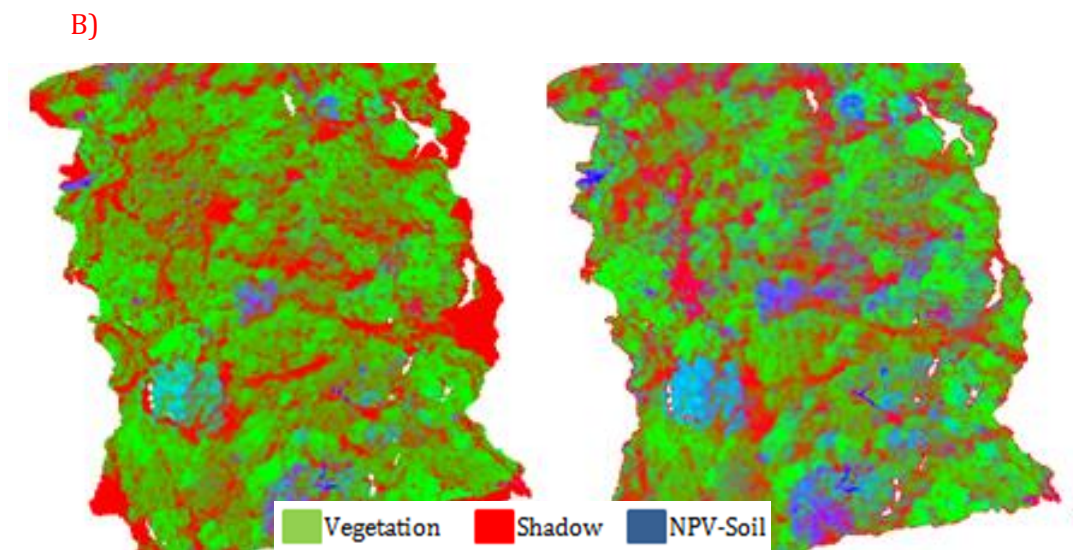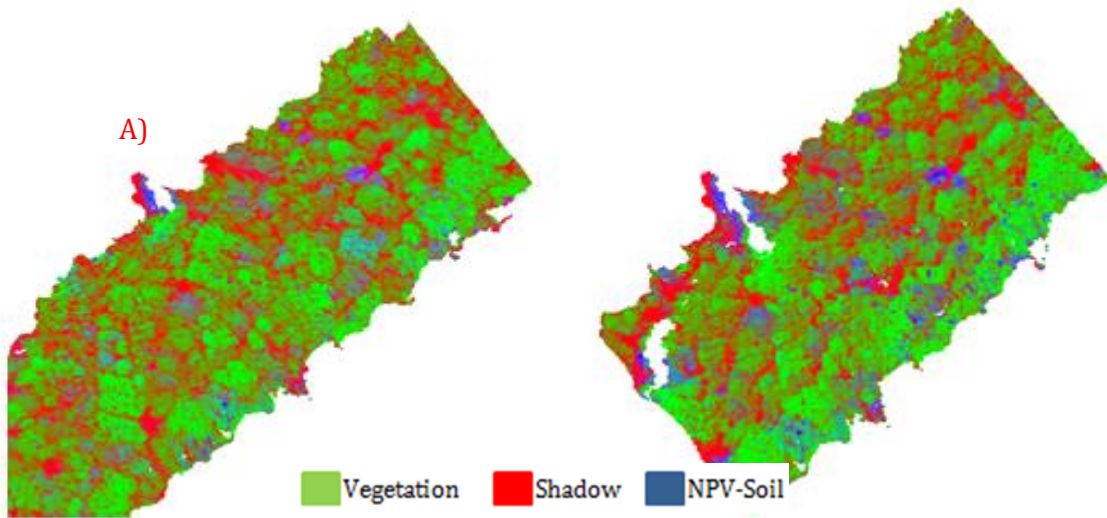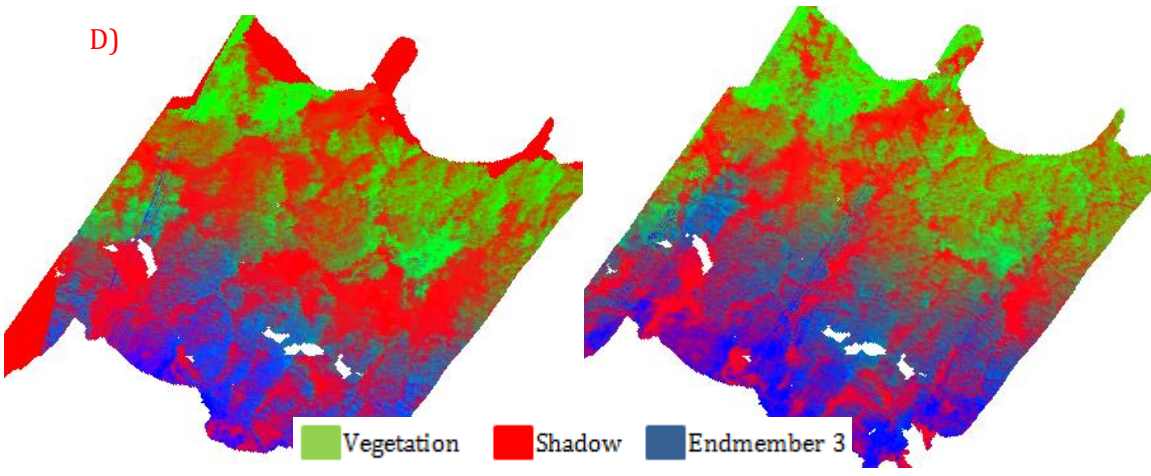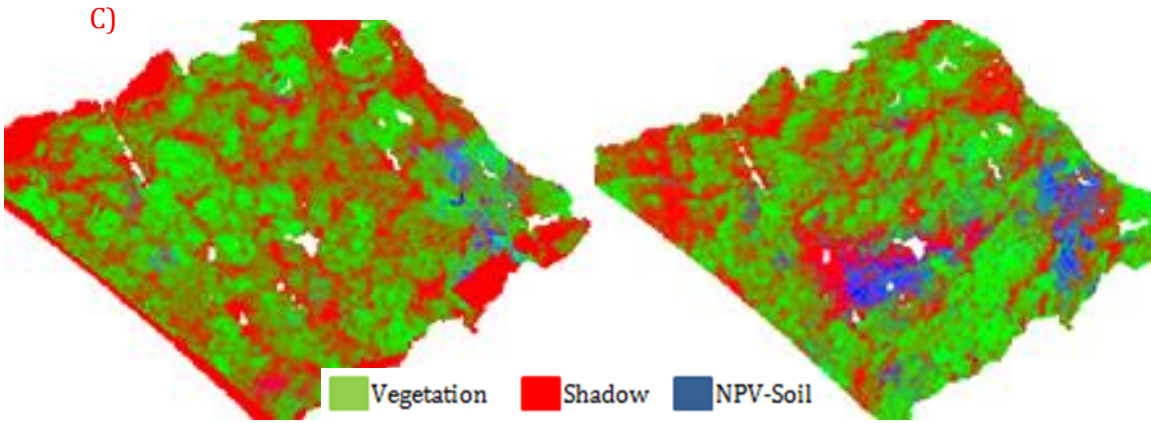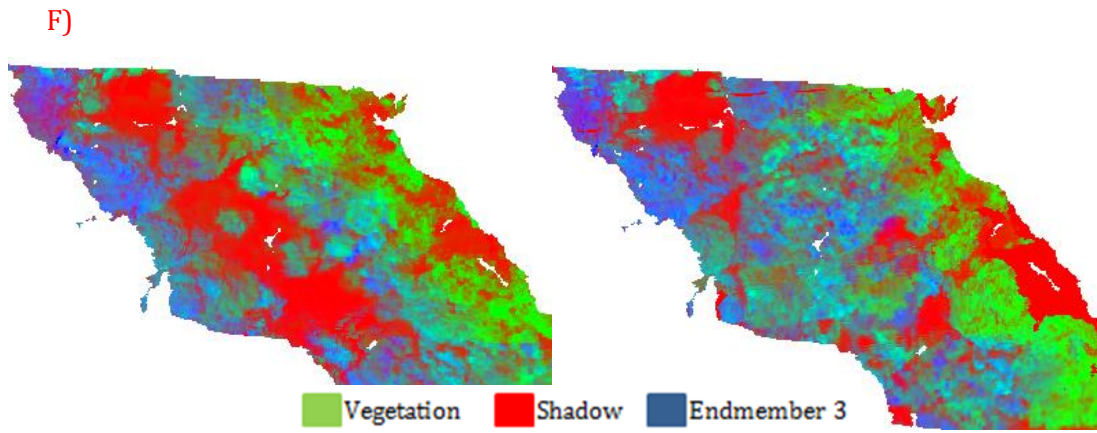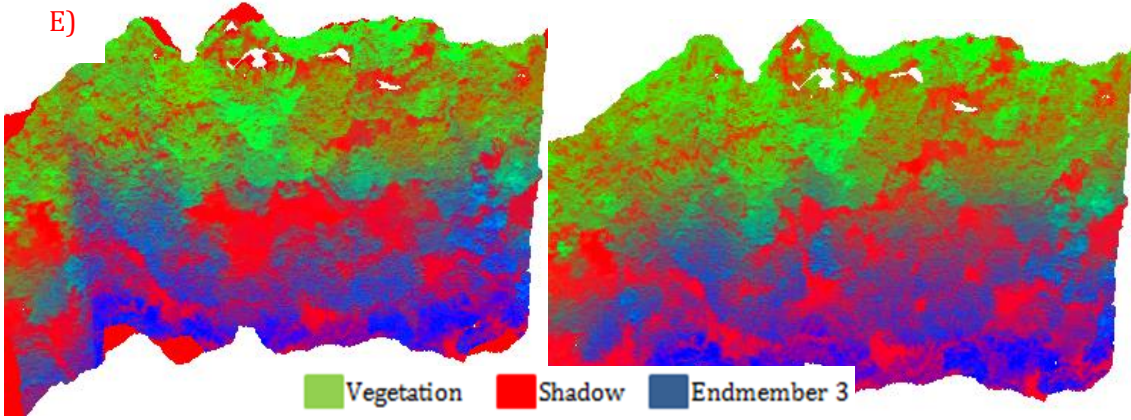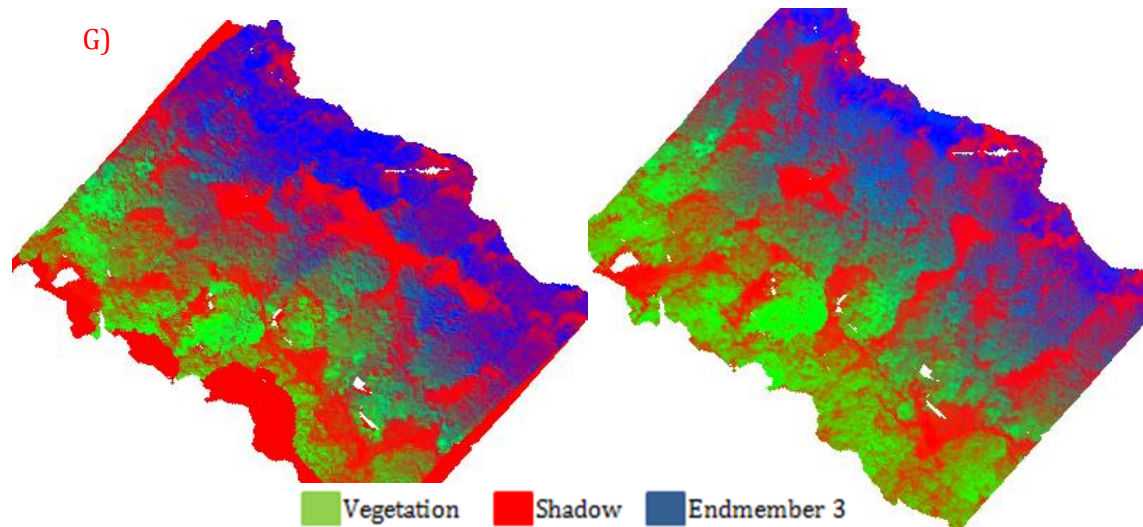
Figure 27. Abundance maps derived from the SMACC algorithm. A) Indonesia plot 2 pre (left) and post-harvest (right), B) Indonesia plot 8 pre (left) and post-harvest (right), C) Indonesia plot 11 pre (left) and post-harvest (right), D) Guyana plot 6 pre (left) and post-harvest (right), E) Guyana plot 7 pre (left) and post-harvest (right), F) Guyana plot 8 pre (left) and post-harvest (right), G) Guyana plot 10 pre (left) and post-harvest (right). Each color represents high endmember abundance. Green color corresponds to the shadow endmember, red corresponds to vegetation endmember and blue corresponds to endmember 3. Endmember 3, in the Indonesian plots 2, 8 and, 11 (A, B and, C) represents the NPV-Soil endmember whereas in the Guyanese plots 6, 7, 8 and, 10 (D, E, F and, G) represents a second vegetation endmember that was distinguished from the first one. The values for each endmember are ranging from 0 to 1. The endmembers in each pixel are summing up to 1. A endmember value of 0 means that the endmember has not been identified whereas a value of 1 means that the endmember is fully covering the pixel.

Appendix C-Difference Maps

This appendix includes the difference maps derived by the subtraction of the dominant gap type endmember.

C)

D)

E)

F)
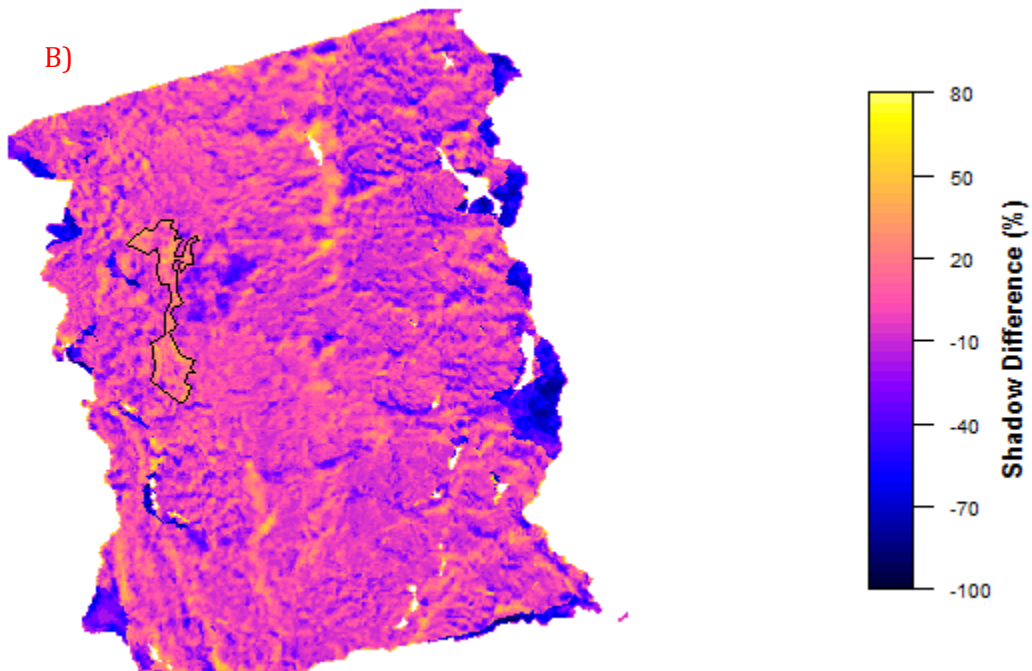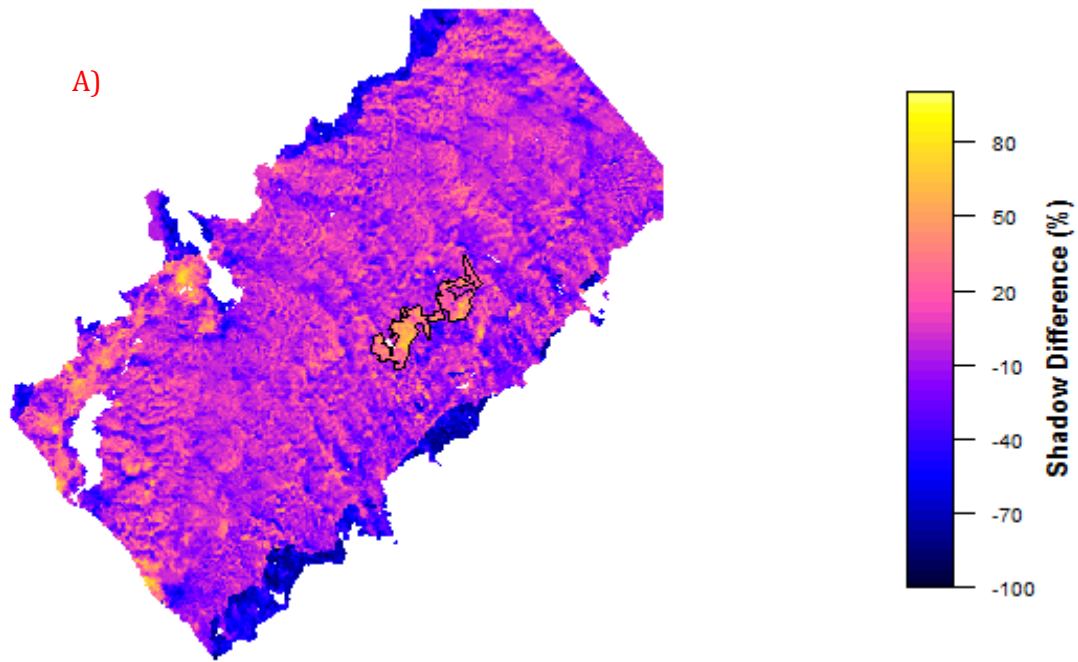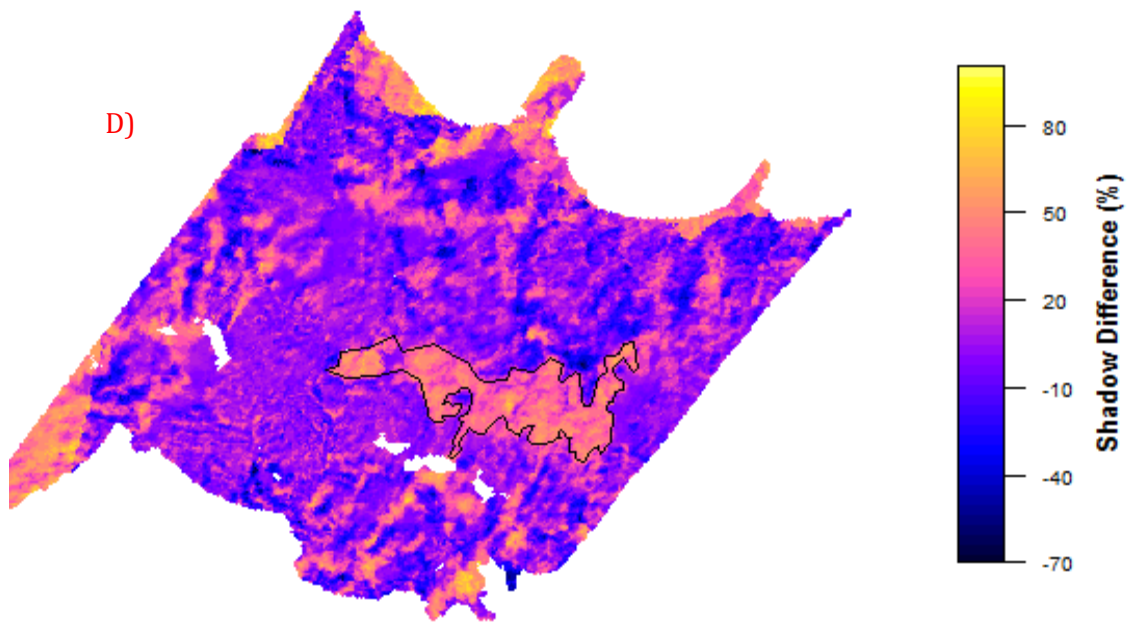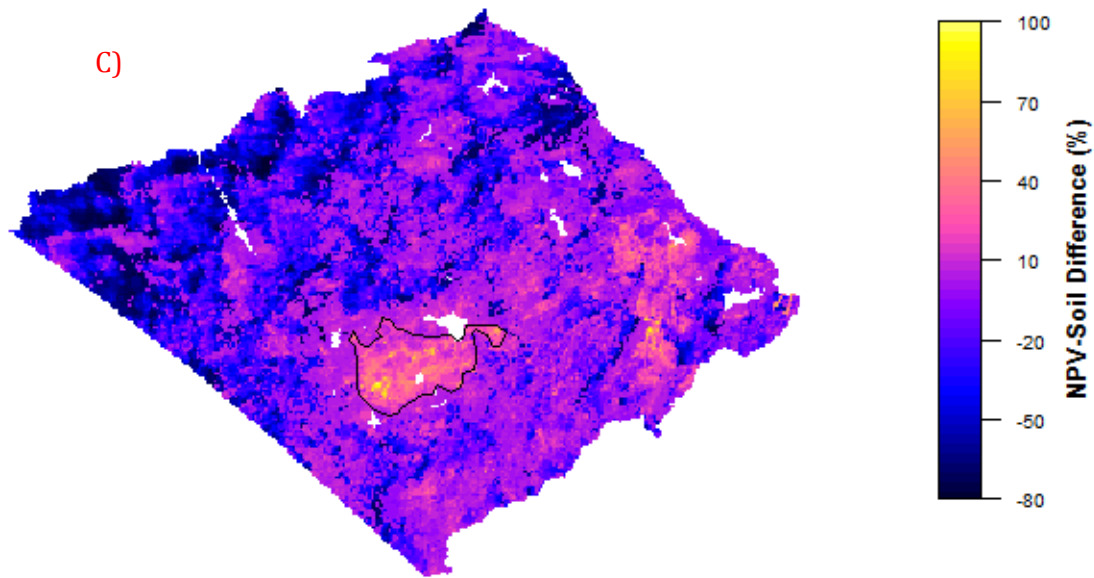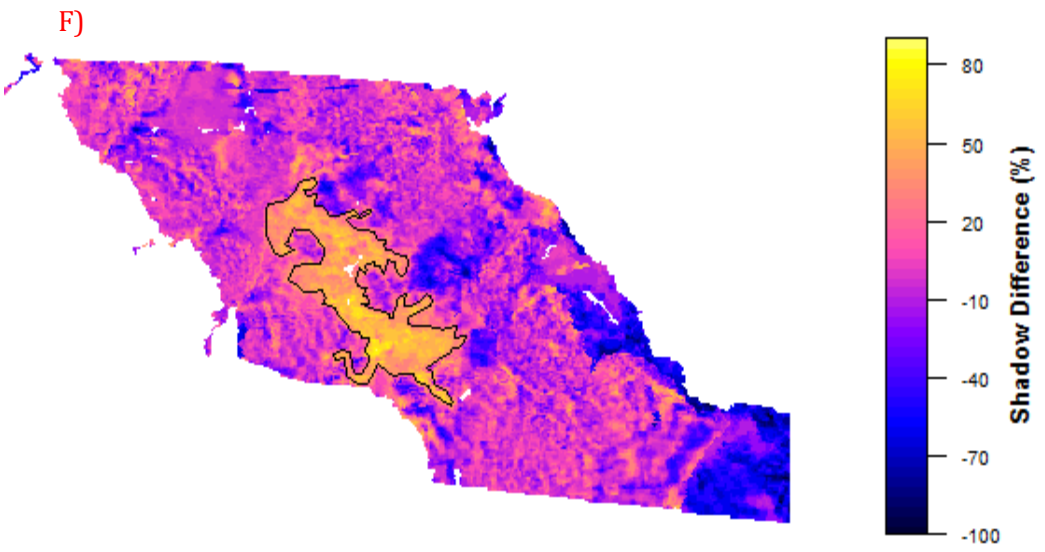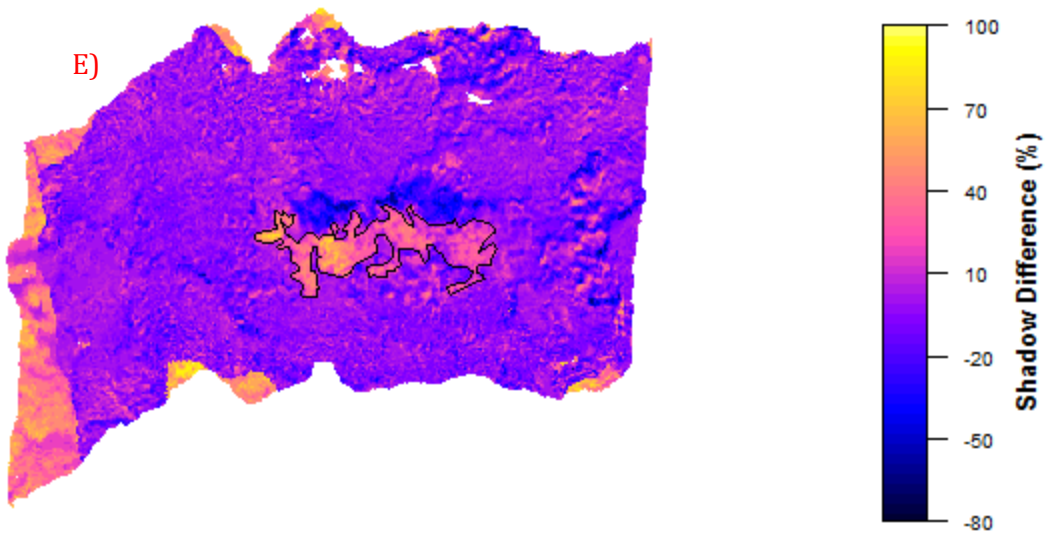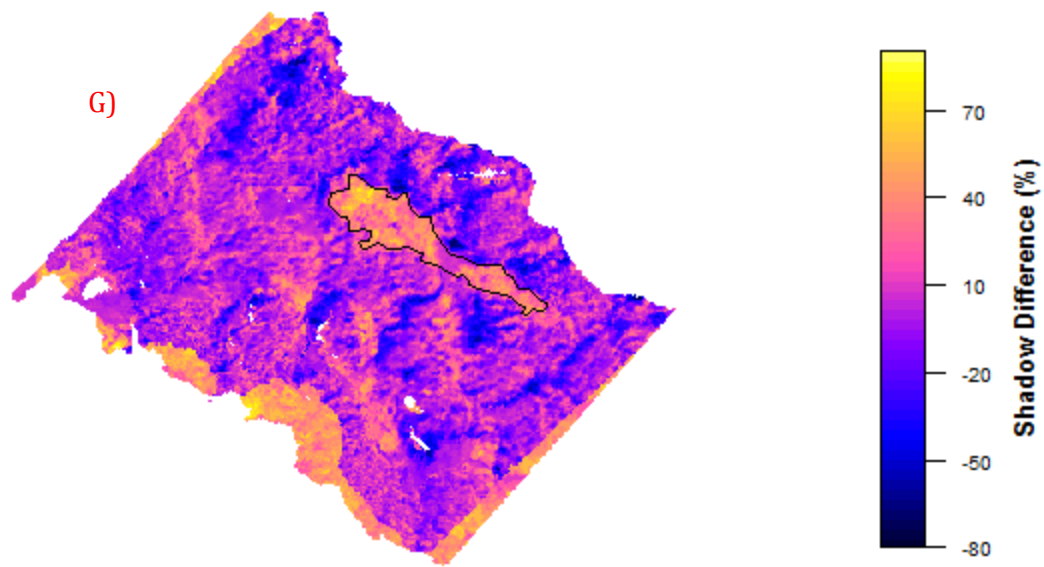
Figure 28. Difference maps of shadow endmember subtraction in Indonesia plot 2 (A), Shadow endmember subtraction in Indonesia plot 8 (B), NPV-Soil endmember subtraction in Indonesia plot 11 (C), and Shadow endmember subtraction in Guyana plots 6, 7, 8, and 10 (D, E, F , and G).